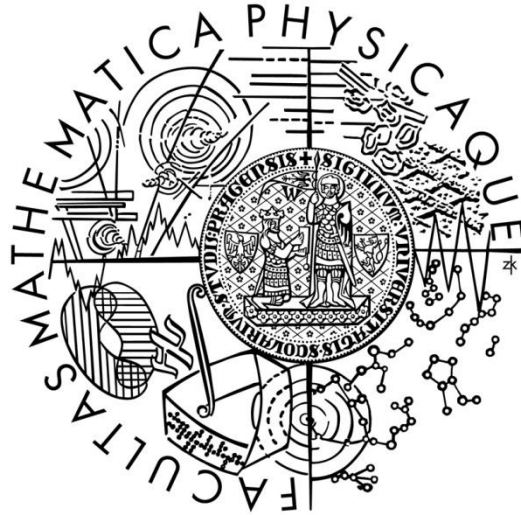


Charles University in Prague
Faculty of Mathematics and Physics



MASTER THESIS

Jakub Zázvorka

Centra rekombinace v semiizolačním CdTe
(Recombination centers in semiinsulating CdTe)

Institute of Physics of Charles University

Supervisor of the master thesis: prof. Ing. Jan Franc, DrSc.

Study programme: Physics

Specialization: Optics and Optoelectronics

Prague 2012

Acknowledgement

This thesis was created with constant support and help of many people.

PD Dr. Michael Fiederle provided support for my study visit in Freiburg, Germany and enabled the use of the TDCM measurement apparatus. Christian Disch adjusted the experimental setup, the measurement control and evaluation program and provided many valuable technological ideas. Dr. Alex Fauler helped to solve many problems during the measurement. The whole service group of material characterization and detector technology at FMF Freiburg created ideal work conditions.

Theory and analysis of the contactless measurement method was done in close cooperation with doc. RNDr. Roman Grill, CSc. Deep level spectroscopy was measured under supervision and advisement of my advisor doc. RNDr. Pavel Hlídaek, CSc. Doc. Ing. Eduard Belas, CSc. , Mgr. Václav Dědič, Bc. Lukáš Šedivý, and other members of the Institute of Physics of Charles University were always there with help when needed.

They all have my sincere thanks.

Special thanks belong to my supervisor prof. Ing. Jan Franc, DrSc. for giving me the opportunity to study and work under his experienced guidance, for creating ideal research conditions, for all comments and precious advice during my work towards the master thesis and for much more.

I acknowledge the support of the foundation Baden-Württemberg-Stiftung in giving me the BW-Stipendium scholarship for my study visit at Albert-Ludwigs-Universität in Freiburg.

I would also like to thank my family and all my friends for their support.

I declare that I carried out this master thesis independently, and only with the cited sources, literature and other professional sources.

I understand that my work relates to the rights and obligations under the Act No. 121/2000 Coll., the Copyright Act, as amended, in particular the fact that the Charles University in Prague has the right to conclude a license agreement on the use of this work as a school work pursuant to Section 60 paragraph 1 of the Copyright Act.

In Prague,

Jakub Zázvorka

Název práce: *Centra rekombinace v semiizolačním CdTe*

Autor: *Jakub Zázvorka*

Katedra / Ústav: *Fyzikální ústav Univerzity Karlovy*

Vedoucí diplomové práce: *prof. Ing. Jan Franc, DrSc., Fyzikální ústav
Univerzity Karlovy*

Abstrakt: *Vlastnosti CdTe pro použití jako detektor záření jsou ovlivněny výskytem hlubokých hladin v zakázaném pásu. Tyto hladiny komplikují sběr náboje a účinnost detektoru. Bezkontaktní měření odporu (COREMA) představuje dobrou možnost charakterizace materiálu bez nutnosti nanášet kovové kontakty. Tato metoda časově závislého měření náboje byla prozkoumána na upravené aparatuře ve FMF Freiburg. Spočítáním teoretických modelů byl stanoven pravděpodobný model založený na zahýbání energetických pásů na povrchu vzorku a neexponenciální závislost transportu náboje v bezkontaktním měření. Jejich pomocí byly vysvětleny tendence výsledků měření a jejich možná spojitost s hlubokou pastí nebo rekombinačním centrem. Byla nalezena korelace mezi odporem, fotovodivostí a fotoluminiscencí pozorované hladiny v blízkosti středu zakázaného pásu. Profily parametrů byly vysvětleny teorií posuvu Fermiho meze relativně k hladině blízko středu zakázaného pásu. Na vzorcích vypěstovaných na MFF UK byly pozorovány tři hluboké hladiny, jejichž fotoluminiscence podporuje prezentovanou teorii a koreluje s profily odporu a infračervené fotovodivosti.*

Klíčová slova: *CdTe, bezkontaktní měření, fotovodivost, fotoluminiscence, hluboké hladiny*

Title: *Recombination centers in semiinsulating CdTe*

Author: *Jakub Zázvorka*

Department / Institute: *Institute of Physics of Charles University*

Supervisor of the master thesis: *prof. Ing. Jan Franc, DrSc., Institute of Physics of
Charles University*

Abstract: *The properties of CdTe for application as a radiation detector are influenced through the presence of deep levels in the band gap. These energy levels complicate the charge collection and the detector efficiency. Contactless resistivity mapping (COREMA) represents a good option for material characterization without the necessity of metal contacts application. The time-dependent charge measurement was investigated on an adjusted apparatus in FMF Freiburg. Theoretical model of charge transport based on band bending on the sample surface was proposed and a non-exponential behavior was calculated. Using this, the resulted parameter tendencies and their connection with deep level trap or recombination center were explained. A correlation was observed between resistivity, photoconductivity and a near midgap level photoluminescence. Parameter profiles were explained using the theory of Fermi level shift relative to the near midgap level. Three deep levels were observed on samples grown at the Charles University in Prague. Their photoluminescence supports the presented theory and correlates with the resistivity and infrared photoconductivity profiles.*

Keywords: *CdTe, contactless measurement, photoconductivity, photoluminescence, deep level*

Contents

1	Introduction	1
1.1	CdTe, CdZnTe	1
1.2	Goal of the thesis	3
2	Theory	4
2.1	Shockley-Read-Hall recombination model	4
2.2	Compensation	7
2.3	Photoluminescence	9
2.4	Photoconductivity	10
2.5	Charge collection	11
2.6	Contactless method of resistivity measurement	14
3	Experimental setup	21
3.1	Contactless resistivity measurement	21
3.2	Photoluminescence	23
4	Results	25
4.1	Adjusting the experiment setup	25
4.2	Contactless resistivity measurement method evaluation	25
4.3	Resistivity dependence on time delay between pulses	31
4.4	Resistivity dependence on frequency	38
4.5	Resistivity and photoconductivity	45
4.6	Resistivity, photoconductivity and deep level spectroscopy correlation	54
5	Conclusion	64
6	References	65
7	List of Tables	68
8	List of Symbols and Abbreviations	69

1 Introduction

Semiconductor materials can be used as radiation detectors using the inner photoelectric effect or Compton effect. One-component materials (silicon, germanium) were thoroughly studied and are used as detectors and electronic devices. Their main disadvantage is a lower atomic number resulting in a small attenuation of high energy photons and a smaller band gap. These types of detectors must be therefore usually cooled down to work properly.

Many other semiconductors are studied due to applications in photoelectric devices (photodetectors, photovoltaics, opto-electrical devices etc.). The two- or three-component compounds of III-V or II-VI are frequently used to fabricate materials with individual properties adjusted to the specific application.

Some compounds, such as CdTe and CdZnTe, can be used as a room temperature x-ray and gamma-ray detectors with a good signal-to-noise ratio, see Ref. [1].

1.1 CdTe, CdZnTe

Cadmium Telluride has a relatively high atomic number Z . The absorption of high-energy radiation by photoelectric effect depends on 4-5 order of magnitude of Z .

The band gap is high enough for the material to be used as a detector at room temperature.

atomic number	$Z_{\text{Cd}}=48$ $Z_{\text{Te}}=52$
band gap energy	1.45eV
lattice constant	6.48 Å
density	$\sim 6 \text{ g}\cdot\text{cm}^{-3}$
effective mass of electrons (holes)	0.11 m_{e0} (0.6 m_{e0})

Table 1 *Properties of CdTe at 300K, Ref. [2]*

The basic requirements for a radiation detector are high resistivity (to improve the s/n^1 ratio) and high mobility-lifetime product. CdTe can be grown as a highly resistive material using the process of compensation. A near midgap deep level is either inserted into the band gap by doping or is naturally present due to native defects or their complexes. Its role is to compensate the concentration difference between the ionized shallow donors and acceptors. Resistivity in the order $10^9-10^{10} \Omega cm$ can be achieved (Ref. [3]). However any energy states in the band gap can act as recombination centers or traps and can effectively worsen the charge collection efficiency of the material. Therefore a study of deep energy levels and identification of their origin can be significant for a production of high quality radiation detectors.

There are many options for deep level investigation, e.g. termo-electric effect spectroscopy (*TEES*), deep level transient spectroscopy (*DLTS*), photoinduced current spectroscopy (*PICTS*), thermally stimulated currents (*TSC*) etc., see Ref. [4]-[6].

Studies have shown (e.g. Ref. [7], [8]) that the surface treatment of CdTe plays a vital role in modification of device properties and can be applied for various applications of the material. The role of the surface states in CdTe-based compounds has been studied e.g. in Ref. [9].

The three-component compound CdZnTe has a higher band gap energy and its use as a radiation detector has been described e.g. in Ref. [10].

The characterization of the material properties can be made using various experiments e.g. the charge collection efficiency measurement. In Ref. [11] a photocurrent measurement was analyzed to determine the mobility-lifetime product. These measurements are done using electrical contacts on the sample. However, contacting can cause structural changes of the interface layer, and in result also the properties of the metal/CdTe/metal structure. In order to characterize only the properties of the CdTe or CdZnTe material contactless methods are optimal. Among them contactless resistivity measurement COREMA (also called the “Time dependent charge measurement”) is widely used.

This method is described in Ref. [12]. A modified setup, as described in Ref. [13], can be used to measure contactless photoconductivity.

¹ signal-to-noise ratio

1.2 Goal of the thesis

The first aim of the master thesis is to design an upgrade of the contactless resistivity measurement apparatus. Resistivity and photoconductivity of CdTe samples should be investigated under higher voltage application and other different parameter setups. The theory of the measurement method should be closely studied. The results are to be analyzed depending on the set parameters.

Using the photoluminescence and deep level spectroscopy measurement regions of samples with different recombination rate (observed by contactless resistivity and photoconductivity mapping) should be assessed. The main goal of the master thesis is to compare the deep level spectroscopy, resistivity and photoconductivity measurement and determine a correlation between them. Depending on this the factors influencing the recombination rate in semiinsulating CdTe are to be specified.

2 Theory

2.1 Shockley-Read-Hall recombination model

The Shockley-Read-Hall recombination model describes the statistics of electron and hole recombination and generation in semiconductors. It was introduced in 1952 in two Physical Review letters (Ref. [14], [15]).

Due to the periodicity and crystal structure of atoms in semiconductors the energy levels that one charge-carrier can have form bands. Last band fully filled is called the valence band and in the higher energies it is followed by a band of forbidden energy states called the band gap. Next band is called the conduction band. The width of the band gap varies from one semiconductor to another. In semiconductors, if an electron is emitted from the valence band a vacant state remains there. This state is also electrically active, can move within the energy band, has an inverse charge and is called a hole.

If there are some impurities or mechanical defects in a semiconductor, the band structure is disrupted and additional allowed energy states can be formed in the band gap, where charge-carriers can be trapped. If the level is far away from the Fermi energy on which the presence probability of an electron occupation is 50% it is called a shallow donor or acceptor; otherwise we speak of deep levels. These are furthermore called recombination centers if the trapping probability of an electron and a hole are equal. If trapping probability of one carrier type dominates, we speak of traps.

The statistics of the trapping mechanism is given in Ref. [16].

We assume one energy level inside the band gap with the concentration N_t and energy E_t . The trapping cross-section will be S_e and S_h for electrons and for holes, respectively. The concentration of already trapped electrons on the deep level is n_t . Because the electrons can be trapped only on an empty state of the deep level, the trapping rate of an electron on the deep level can be expressed as

$$S_e v_e (N_t - n_t) n = \gamma_e (N_t - n_t) n \quad (1)$$

Here v_e is the speed of the electron and n is the concentration of free electrons.

Otherwise the holes can only be trapped on a deep level state filled with an electron, therefore the trapping rate of holes is

$$S_h v_h n_t p = \gamma_p n_t p \quad (2)$$

Here v_h is the hole speed and p the concentration of holes.

Trapping of the charge carrier is not the only process taking place in the band structure. The trapped carrier can be thermally released back to the conduction or valence band, with the probability α_e and α_h respectively for electrons and holes.

In thermodynamic equilibrium (with the values subscripted with 0), we can write

$$\frac{dn_0}{dt} = \alpha_e n_{t0} - \gamma_e (N_t - n_{t0}) n_0 \quad (3)$$

Because in the equilibrium the free electron concentration does not change, we can write

$$n_{t0} = \frac{N_t}{\frac{\alpha_e}{\gamma_e n_0} + 1} \quad (4)$$

Electrons follow the Fermi-Dirac distribution function

$$n_{t0} = N_t f = \frac{N_t}{\exp\left(-\frac{E_F + E_t}{kT}\right) + 1} \quad (5)$$

Here k is the Boltzmann constant and T is the temperature.

If we compare the equations (4) and (5) and use the Fermi-Dirac distribution for the free electrons $n_0 = N_C \exp\left(\frac{E_F}{kT}\right)$, where N_C are the states in the conduction band, we obtain

$$\alpha_e = \gamma_e N_C \exp\left(-\frac{E_t}{kT}\right) \quad (6)$$

Therefore

$$\alpha_e n_t = \gamma_e N_C n_t \exp\left(-\frac{E_F}{kT}\right) = \gamma_e n_t n_1 \quad (7)$$

where n_1 stands for the concentration of electrons in the case of the Fermi level being pinned to the deep level.

Simultaneously for holes the following equation is valid

$$\alpha_h(N_t - n_t) = \gamma_h(N_t - n_t)p_1 \quad (8)$$

Now we get the differential equations for the trapping process

$$\frac{dn}{dt} = G + \gamma_e n_t n_1 - \gamma_e(N_t - n_t)n \quad (9)$$

$$\frac{dp}{dt} = G + \gamma_h(N_t - n_t)p_1 - \gamma_h n_t p \quad (10)$$

$$\frac{dn_t}{dt} = \gamma_e(N_t - n_t)n - \gamma_h n_t p - \gamma_e n_t n_1 + \gamma_h(N_t - n_t)p_1 \quad (11)$$

where G is the charge generation rate.

The trapped electron has two options, to recombine with a hole or to be thermally excited to the conduction band. If the trapping cross-sections of both charge carriers are similar, the hole is trapped quickly, the electron does not have to wait and both carriers recombine; the deep level works as a recombination center. If the electron trapping cross-section is bigger than the hole cross-section, the electron has to wait for a hole to be trapped and it is likelier that it is thermally excited back to the conduction level. The level then works as an electron trap, as mentioned above.

The trapped carriers cannot contribute to the electrical current in the material and if the semiconductor is used as a radiation detector, the deep level influences the charge collection efficiency and other material properties.

2.2 Compensation

As mentioned above, for the use of CdTe as a radiation detector with good signal-to-noise ratio, it is necessary to have a high resistivity material. The intrinsic resistivity of CdTe is about $10^9 \Omega cm$ and normally it is not possible to grow a perfectly pure crystal without any defects. These defects (both native defects and foreign impurities) form both donor or acceptor states in the band gap. Undoped material is typically low-resistivity p-type due to formation of Cd vacancies that act as acceptors. To achieve the high resistivity, the concentration of shallow donor and acceptor levels has to be nearly equal. A deep, near midgap level, which compensates the difference between the shallow level concentrations is introduced into the material. The mechanism of compensation is described in Ref. [3] and subsequently in Ref. [13].

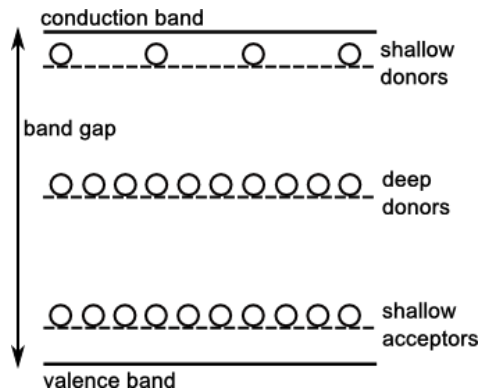


Fig. 1 *Initial state of compensation process, all levels are neutral*

Assuming the material has a shallow donor concentration N_D , shallow acceptor concentration N_A , deep level concentration N_{DL} and assuming

$$N_D < N_A \quad (12)$$

the donor electrons will recombine with the acceptor holes. The donors will be fully ionized, but the acceptors will be only partially ionized, as shown in **Fig. 2**. Now the semiconductor is a lower resistivity p-type.

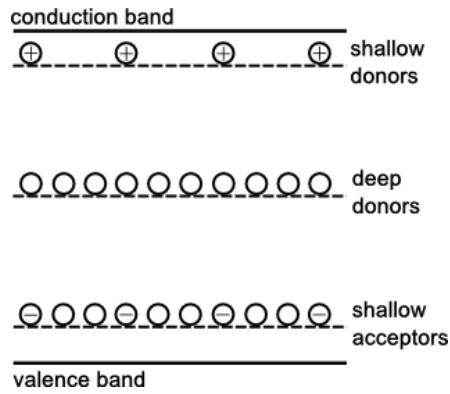


Fig. 2 *Compensation process, partially ionized acceptors*

The spontaneously emitted electrons from the deep donors will recombine with the acceptors, so that the acceptors become fully ionized, if

$$N_A - N_D < N_{DL} \quad (13)$$

and the deep level becomes partially ionized, see **Fig. 3**.

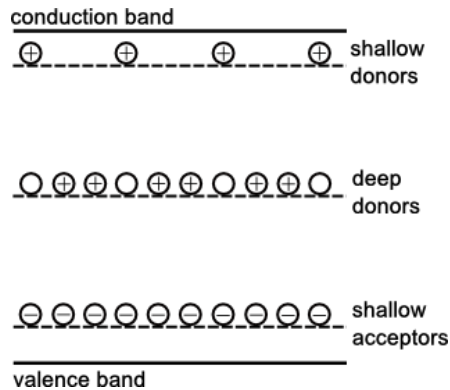


Fig. 3 *Compensation process, partially ionized deep donors*

Now the electric neutrality equation is fulfilled, free electrons can only be emitted from the neutral state of the deep level, which is the same as if the Fermi level would be at the deep level energy.

2.3 Photoluminescence

Photoluminescence is a characterization method often used to study semiconductors. It is a luminescence caused by absorption of photons. The incoming photons give their energy to electrons in the valence band, thus exciting them to a higher energy state, which is mostly in the conduction band. Now the electrons find themselves in thermo dynamical non-equilibrium and move back to the initial state. The energy they have can be emitted again as a photon or it can be transferred to the crystal lattice in the form of phonons, see **Fig. 4**.

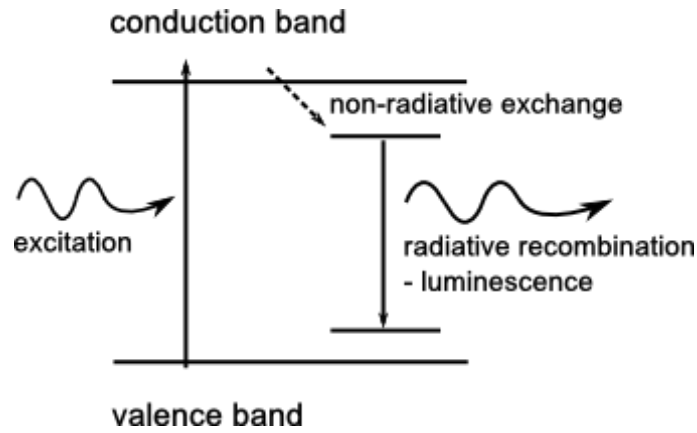


Fig. 4 *Basic luminescence scheme in a semiconductor*

To describe the dynamics of the process an average time of this energy exchange is introduced as τ_{nr} for the exchange with the lattice and τ_r for the return to the initial state with the photon emission, as described in Ref. [17]. The reciprocal value of this variable gives the probability of the transition over a period of time. The overall probability will be

$$\frac{1}{\tau_g} = \frac{1}{\tau_{nr}} + \frac{1}{\tau_r} \quad (14)$$

According to this a differential equation for the electrons can be written as

$$\frac{dn}{dt} = G - \frac{n}{\tau_g} \quad (15)$$

where G stands for the generation of the electron by absorbing the energy of photons incoming from an external illumination source.

The emitted photons created by the radiant exchange have energy equal to the energy difference between the excited and initial state. These photons can be focused into a spectrometer and their energy can be evaluated. This is a means to study the energy levels in the semiconductor.

2.4 Photoconductivity

If a semiconductor material is illuminated, electrons can be emitted from the initial state into the conduction band. It changes the equilibrium concentration and charge carriers are generated. When the illumination energy is high enough (at least as the band gap) electrons can be emitted from the valence band. The charge carrier concentration changes in both the valence and conduction bands.

$$\begin{aligned} n &= n_0 + \Delta n \\ p &= p_0 + \Delta p \end{aligned} \tag{16}$$

Here the n, p are the electron and hole concentrations in valence and conduction band, respectively. Equilibrium concentrations are n_0, p_0 and $\Delta n, \Delta p$ are the concentration of charge carriers generated by the illumination.

Charge carriers can also be generated from impurity states in the band gap (shallow donors or acceptors).

The main equation for the charge transport in semiconductors is the drift-diffusion equation (here written for electrons).

$$j = e n \mu_n E + k T \nabla n + e S_n \nabla T \tag{17}$$

The first part of the equation determines the drift. Here e is the electron charge, n is the electron concentration, μ_n the mobility of the electron, E the electrical field applied to the semiconductor. The diffusion is described in the second part of the equation with k as the Boltzmann constant and T as the temperature. The final part of the equation describes the Soret effect with the Soret coefficient S_n . This effect is usually neglected in the calculations.

The drift part of the equation can be rewritten using a relation for the conductivity

$$\sigma_n = e n \mu_n \quad (18)$$

as

$$j_{n_{drift}} = \sigma_n E \quad (19)$$

This is the formulation of Ohm's law.

If we apply voltage to a semiconductor and illuminate it afterwards, we can see a change in the conductivity of the material. This is because of the additional charge carriers, which can contribute to the conductivity.

$$\begin{aligned} j_{n_{drift}} &= e (n_0 + \Delta n) \mu_n E = e n_0 \mu_n E + e \Delta n \mu_n E \\ j_{n_{drift}} &= j_{n_0_{drift}} + j_{\Delta n_{drift}} \end{aligned} \quad (20)$$

The conductivity caused by the additional charge carriers generated with the illumination is called photoconductivity. Depending on the initial state of the generated charge carriers we can have band gap photoconductivity, where both types of carriers mostly have the same concentration and contribute equally to the conductivity. Or we can have impurity state photoconductivity, where only one type of charge carriers is contributing. The impurity photoconductivity requires lower energy of the illumination for the additional charge carriers to be generated.

Because the amount of carriers generated with the illumination Δn depends on the photon flow Φ and can be expressed using the carrier lifetime τ

$$\Delta n = \frac{\eta \tau_g \Phi}{w A} \quad (21)^2$$

this phenomenon can be used to measure the incoming light intensity.

2.5 Charge collection

To characterize the ability of a material for use as a photodetector the charge collection efficiency is used. This is the outcome of the so called Hecht equation,

² η is the wavelength dependable ratio of absorbed and incoming photons
 $w A$ is the volume illuminated volume of the material

Ref. [18]. The derivation of the Hecht equation uses the Shockley-Ramo theorem, Ref. [19].

Let us assume a planar detector, biased with voltage U , with the distance between the contacts L . As a result of illumination charge carriers are generated. If the negative contact is illuminated electrons will drift through the detector towards the positive contact. On their way, they can recombine.

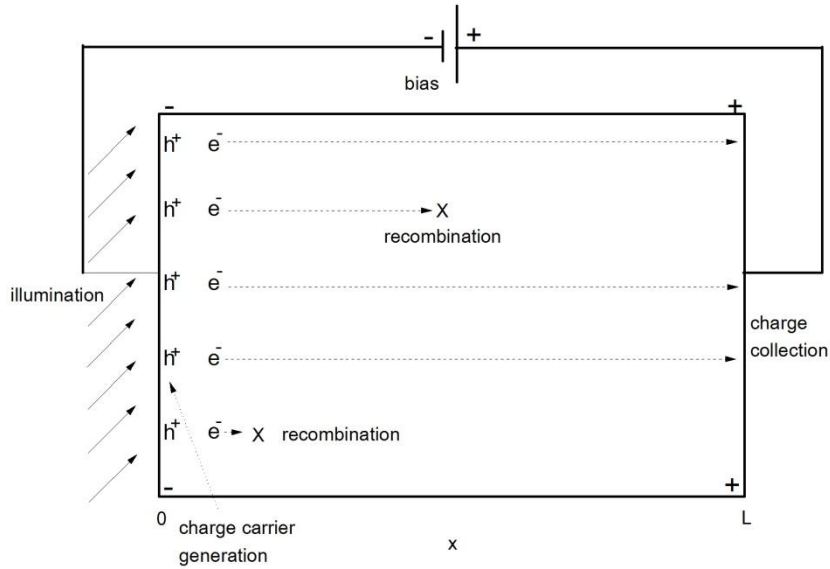


Fig. 5 *Schematic of the charge collection in a photodetector*

The moving carriers will have the velocity

$$v = \mu \frac{U}{L} \quad (22)$$

If we set the x coordinate origin in the negative contact (see **Fig. 5**) and the carriers are generated in $t = 0$, after time t they will have moved to

$$x = vt \quad (23)$$

On this way the charge carriers will be trapped and depending on the coordinate x the remaining charge carriers will be

$$q(x, t) = q_0 \cdot e^{-\frac{t}{\tau_g}} \quad (24)$$

where τ_g is the lifetime of the carriers.

Integrating the charge through the detector (till the time $= \frac{L^2}{\mu U}$, when the charge carriers reach the electrical contact) and assuming the voltage in the detector to be constant, we get the ratio of collected charge to the charge generated.

$$\frac{Q}{Q_0} = \frac{\mu\tau U}{L^2} \left(1 - e^{-\frac{L^2}{\mu\tau_g U}} \right) \quad (25)$$

Measuring the charge collection with different bias voltages allows determining the $\mu\tau_g$ product. This is a valuable characterisation parameter for the ability of the material to be used as a radiation detector.

The connection between the photoconductivity and charge collection has been described in Ref. [11]. Here the photocurrent has been approximated with Hecht's relation.

Toney et al. (Ref. [20]) have used photocurrent mapping for study of the charge transport properties and the distribution of the electrical field in CdZnTe.

2.6 Contactless method of resistivity measurement

The contactless measurement of a sample resistivity by using time-dependent charge measurement is a method first developed at the Fraunhofer Institute for material science in Freiburg, Germany. The first paper published about this measurement was by R.Stibal in 1991 (Ref. [12]).

The sample resistivity can be determined without the need of preparation of ohmic contacts on the sample, which are otherwise necessary, e.g. for Hall measurements. The resistivity evaluation uses only relative units. Therefore there are no specific requirements for the sample, only a certain level of flatness of the samples in the mapping mode of the measurement. Samples with resistivity from 10^6 to $10^{11} \Omega cm$ can be measured using the time-dependent charge measurement.

It is shown in **Fig. 6** that the results of this method have a very good correlation with the Hall measurement, in the van de Pauw mode. The presented measurement was performed on GaAs samples.

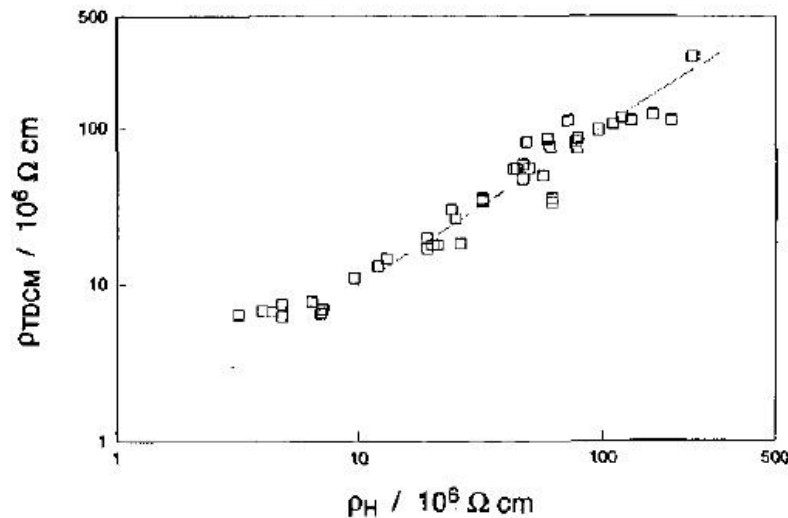


Fig. 6 *Correlation between resistivity ρ_{TDCM} measured by the TDCM technique with van de Pauw Hall data ρ_H , Ref. [12]*

Basic layout of the experiment is shown in **Fig. 7**. The setup consists of a back electrode on which the sample is placed. Over it is the measuring electrode (here called probe or sensor) with a guard ring to homogenize the electric field in the measuring point.

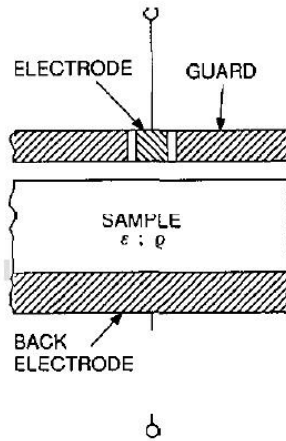


Fig. 7 *Basic layout of the experiment, Ref. [12]*

Between the sample and the probe is an air gap, according to Ref. [12] usually about $0,1\text{mm}$ thick. This gap can be visualized in the electric scheme as a capacitor with the capacity C_A . The sample then has a capacity C_S and resistance R_S in a parallel connection to each other and in a serial connection to the air gap capacity.

The equivalent scheme is shown in **Fig. 8**.

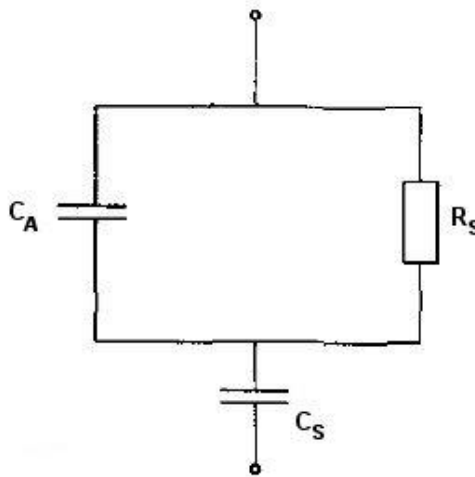


Fig. 8 *Equivalent arrangement of the electrical circuit of the measurement, Ref. [12]*

The characteristics of this scheme can be calculated using Kirchhoff's laws and the Laplace transformation.

In accordance to Kirchhoff's second law we know that the voltage on the source U_Z is the voltage in the layout, in this case the sum of the voltages on the sample U_S and on the air gap U_A .

$$U_Z = U_{C_A} + U_S \quad (26)$$

The voltage on the sample remains the same

$$U_S = U_{R_S} = U_{C_S} \quad (27)$$

Simultaneously the current flowing out of the sample must be the current on the air gap

$$I_{C_S} + I_{R_S} = I_{C_A} \quad (28)$$

For the resistance and capacitor voltages the following equations apply

$$U_R = I_{R_S} \cdot R_S \quad (29)$$

$$U_{C_i} = \frac{1}{C_i} \int I_{C_i} \quad (30)$$

Using (26) and (30) the voltage on the source can be rewritten to

$$U_Z = \frac{1}{C_A} \int I_{C_A} + U_S \quad (31)$$

which with (28) and (29) gives

$$U_Z = \frac{1}{C_A} \int \left(C_S \frac{\partial U_{C_S}}{\partial t} + \frac{U_{R_S}}{R_S} \right) dt + U_S \quad (32)$$

According to (27) the voltages are equal, therefore

$$U_Z = \frac{1}{R_S C_A} \int U_S dt + \left(1 + \frac{C_S}{C_A} \right) U_S \quad (33)$$

The voltage is applied in the form of rectangular pulses with the height U_0 and the on-time T_{HIGH} and off-time T_{LOW} . We assume the beginning of the pulse in the time $t=0$. The illustration of the pulses is presented in **Fig. 9**. U_z can be written as

$$U_Z = U_0 \cdot \Theta(t) - U_0 \cdot \Theta(t - T_{HIGH}) \quad (34)$$

Here $\Theta(t)$ is the Heaviside function.

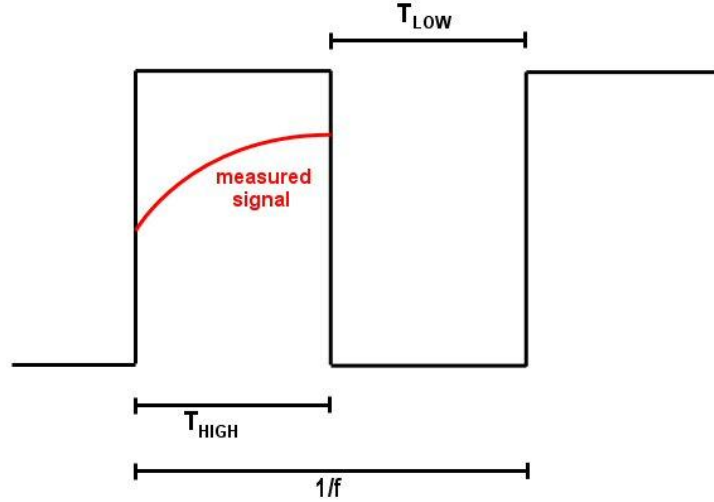


Fig. 9 Labeling and scheme of the applied pulses

If we set (33) and (34) equal and use the Laplace transformation via formulas written in Ref. [21] on the equation, we get

$$\frac{U_0}{p} (1 - e^{-pT_{HIGH}}) = \left(\frac{1}{R_S C_A} \cdot \frac{1}{p} + \left(1 + \frac{C_S}{C_A} \right) \right) \cdot U_S \quad (35)$$

This can be rewritten to a better form for the reverse Laplace transformation

$$U_S = U_0 \cdot \frac{C_A}{C_S + C_A} \cdot \frac{1 - e^{-pT_{HIGH}}}{p + \frac{1}{R_S(C_S + C_A)}} \quad (36)$$

After the transformation we get the formula for the voltage on the sample

$$U_S = U_0 \cdot \frac{C_A}{C_S + C_A} \left(\Theta(t) \cdot e^{-\frac{t}{\tau}} - \Theta(t - T_{HIGH}) \cdot e^{-\frac{t - T_{HIGH}}{\tau}} \right) \quad (37)$$

where τ is the dielectric relaxation constant

$$\tau = R_S(C_S + C_A) \quad (38)$$

The time-dependent charge on the air gap is the difference between the source voltage and the voltage on the sample

$$U_A = U_0 \cdot \left(\left(1 - \frac{C_A}{C_S + C_A} e^{-\frac{t}{\tau}} \right) \Theta(t) - \left(1 - \frac{C_A}{C_S + C_A} e^{-\frac{t-T_{HIGH}}{\tau}} \right) \Theta(t - T_{HIGH}) \right) \quad (39)$$

With the relation

$$Q_i = C_i \cdot U_i \quad (40)$$

We can determine the time-dependent charge on the capacitor of the air gap (for simplicity we from now on assume only the time where the pulse is applied to the circuit).

$$Q_A(t) = U_0 \cdot C_A \left(1 - \frac{C_A}{C_S + C_A} e^{-\frac{t}{\tau}} \right) \quad (41)$$

The equation can be written in the form as published in [12].

$$\begin{aligned} Q_A(t) &= U_0 \left(\frac{C_A C_S}{C_S + C_A} + \frac{C_A^2}{C_S + C_A} \left(1 - e^{-\frac{t}{\tau}} \right) \right) \\ &= Q_A(0) + U_0 \frac{C_A^2}{C_S + C_A} \left(1 - e^{-\frac{t}{\tau}} \right) \end{aligned} \quad (42)$$

Important values are the ones in time origin and infinity

$$Q_A(0) = U_0 \frac{C_A C_S}{C_S + C_A} \quad (43)$$

$$^3 Q_A(\infty) = U_0 C_A \quad (44)$$

Assuming the circuit fully discharged before the measurement, there is a charge built-up with the height according to (43) after the voltage is applied. After that the sample capacitor discharges itself over the sample resistance. In the end there

³ $Q_i(\infty)$ will also be written as Q_{inf}

is no charge on the sample and all of the charge is on the air gap capacitor, which shows the equation (44).

Now the equation for the dielectric constant τ (38), along with (43) and (44) can be put together

$$\tau = R_S U_0 C_A \frac{C_S}{Q_A(0)} = R_S C_S \frac{Q_A(\infty)}{Q_A(0)} \quad (45)$$

And with the relations for resistance and capacity

$$R_S = \rho \frac{d}{S} \quad (46)$$

$$C_S = \varepsilon_0 \varepsilon_r \frac{S}{d} \quad (47)$$

Here ρ is resistivity, $\varepsilon_0, \varepsilon_r$ are permittivity and relative permittivity respectively, S is the area of the resistor or capacitor and d is its width.

Because in our case the resistor and capacitor is the same sample, the areas and widths are the same and using (46), (47) they cancel each other out in the equation (45). Therefore the resistivity of the sample can be calculated from the dielectric constant τ with the equation

$$\rho = \frac{Q_A(0)\tau}{\varepsilon_0 \varepsilon_r Q_A(\infty)} \quad (48)$$

We can see that the resistance is determined by the relative change of charge on the air gap. This is measured with a charge-sensitive amplifier set parallel to the air gap as shown in **Fig. 10**. It gives voltage proportional to the charge on the air gap, which is measured with an oscilloscope and recorded to a computer.

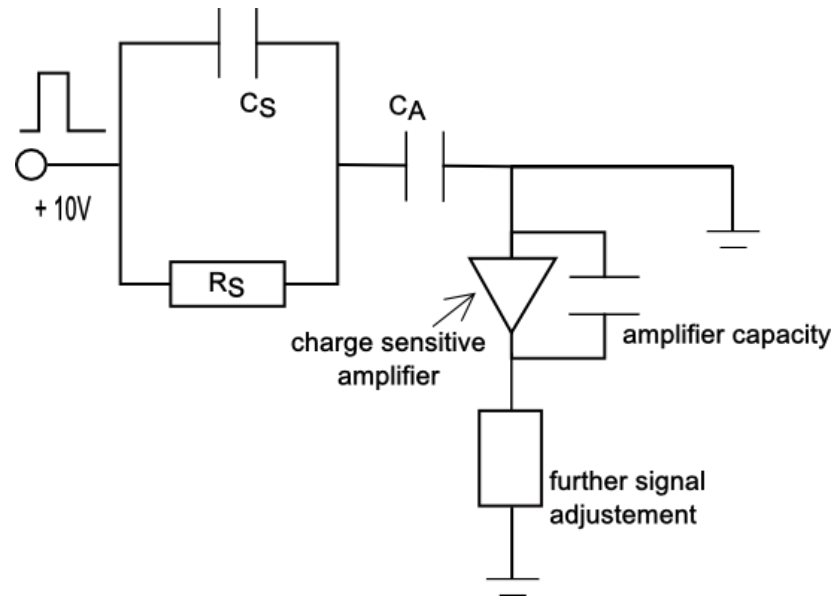


Fig. 10 *Electrical circuit of the TDCM measurement*

The measured signals are evaluated with a fitting function; the charges in origin and infinity are determined, along with the dielectric constant. The fitting function is

$$U_{AMPLIFIER}(t) = U_{AMPLIFIER}(0) + A \left(1 - e^{-\frac{t}{\tau}}\right) \quad (49)$$

In the end the resistance is determined using a modified relation (48)

$$\rho = \frac{U_{AMPLIFIER}(0) \tau}{\varepsilon_0 \varepsilon_r (U_{AMPLIFIER}(0) + A)} \quad (50)$$

3 Experimental setup

3.1 Contactless resistivity measurement

In Prague we used the commercially available COREMA-WT from Semimap Scientific Instruments GmbH, shown in **Fig. 11**. The measurement device is housed in a cca. $50 \times 50 \times 150 \text{ cm}$ box and connected to a computer with the evaluation software. This apparatus is able to measure wafers with diameter up to 150 mm and the thickness up to $5000 \mu\text{m}$. The resistivity measurement range is $10^5 - 10^{12} \Omega\text{cm}$; with the repeatability better than 1% in the range $10^6 - 10^9 \Omega\text{cm}$. The only requirement for the sample is for the lateral thickness to vary less the $20 \mu\text{m}$ for the mapping measurement, which can be done with up to $512 \times 512 \text{ pixels}$. The sensor size is 1 mm in diameter and around it is a guard-ring which homogenizes the electric field in the measuring point.

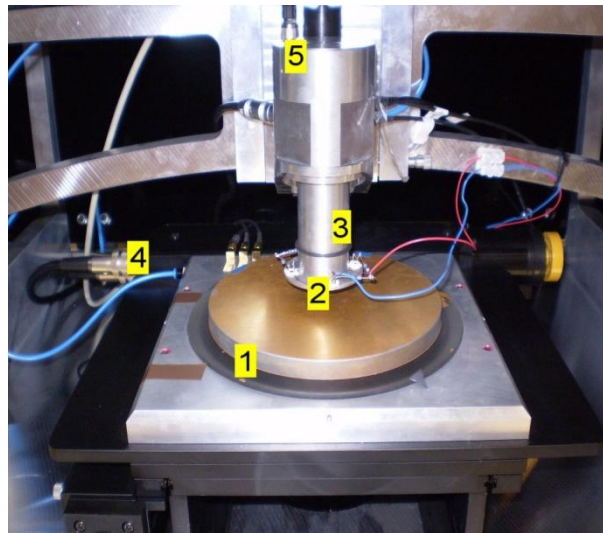


Fig. 11 *Picture of measuring apparatus COREMA-WT:*

1-back electrode, 2-ring with LED diodes, 3-sensor and guard tubus, 4-movement control in x,y axes, 5-z axis positioning control

The single signal measurement can be done with 1024 or 2048 scan points with the time between these points (sweep time) from $0.01 \mu\text{s} - 1310 \mu\text{s}$, which means

that the frequency of the applied pulses can vary from $48kHz$ to $0.2Hz$ and only symmetrical pulses can be applied.

It can be used for GaAs, InP, CdTe, GaN etc.

As a part of Ref. [13] the apparatus was modified to measure photoconductivity. To the sensor tube a ring with LED diodes was attached with individual control and power supply. The ring can be swiftly changed to another one with different LED to vary the wavelength of the external illumination source. Used LEDs and their characteristics are shown in **Table 2** and **Table 3**.

diode	L3989
material	InGaAs
operating temperature T_O	-35 to 85°C
forward current I_F	80mA
reverse voltage V_R	3V
typical peak emission wavelength, $I_F=50mA$	830nm
spectral half width, $I_F=50mA$	40nm

Table 2 *Properties of diode L3989*

diode	ELD-1720-535
material	InGaAs/InP
operating temperature T_O	-20 to 80°C
forward current I_F	100mA
reverse voltage V_R	5V
typical peak emission wavelength, $I_F=20mA$	1720nm
spectral half width, $I_F=20mA$	130nm

Table 3 *Properties of diode ELD-1720-535*

The sample resistivity is measured with and without the illumination and the photoconductivity γ is evaluated using the equation

$$\gamma = \frac{1}{\rho_{light}} - \frac{1}{\rho_{dark}} \quad (51)$$

At FMF Freiburg, basically the same setup is used, but an external pulse generator forms the applied pulses. Parameters of the pulses can be adjusted within the generator, but the pulse voltage can be only $10V$ high. The signal of the sensor is

taken by an oscilloscope and sent to a computer with evaluation software. The evaluation occurs with a LabView program, where the equation (50) is fitted to the measurement. Here photoconductivity can also be measured. One LED diode is placed from the top into the sensor tube and through reflection on the tube wall the light reaches the sample. Due to the better option of setting the measurement parameters, the apparatus is widely used in CdTe characterization, e.g. Ref. [22].

3.2 Photoluminescence

The photoluminescence spectra have been measured in Prague, using the setup shown in Fig. 12.

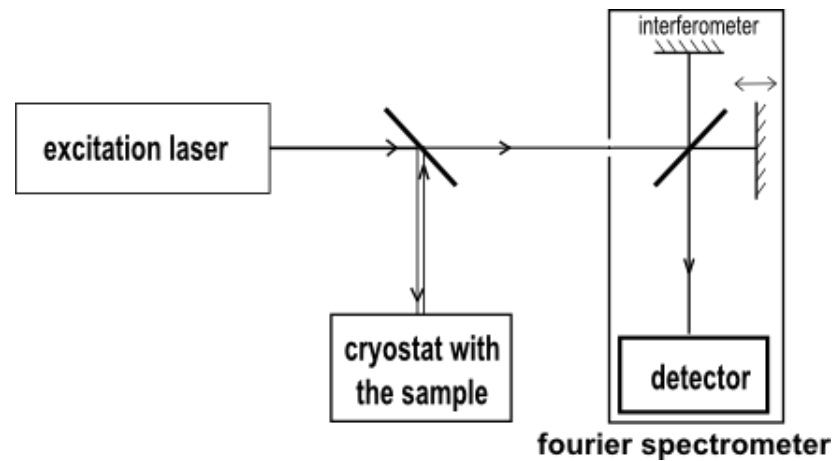


Fig. 12 *Photoluminescence measurement setup*

The sample is placed into a cryostat and using liquid helium it is cooled down to 4.2K. Then it is illuminated with a Radius He-Ne laser ($\lambda=633nm$) or with Spectra Physics 3900S Ti:Sapphire laser (tunable in the range 1.13 – 1.64eV). The photoluminescence spectrum is then filtered from the excitation light and evaluated with Bruker IFS 66/S Spectrometer.

Three detector types are used to read the spectra.

detector material	sensitivity range	working temperature	excitation laser
Si	1.05 – 1.82 eV	295 K	He-Ne
Ge	0.71 – 1.47 eV	77 K	He-Ne
InSb	0.45 – 1.75 eV	77 K	Ti:Sapphire

Table 4 *Detector types and parameters in the PL measurement,*
Ref. [23]

In this measurement, only Si and InSb detectors were used to study the shallow level and deep level energy, respectively. The cryostat is outfitted with a motor driven positioning system with micrometric accuracy. So a photoluminescence mapping of the sample can be done without greater changes in the experiment setup.

4 Results

4.1 Adjusting the experiment setup

We modified the resistivity apparatus in Freiburg. Now the source of the pulses is an external voltage generator, which is connected to the back electrode through STMicroelectronics L298 H-Bridge. With this setup, voltage up to $45V$ can be applied on the apparatus electrodes. The experiment is controlled with a National Instrument Drive Card and thus all parameters can be adjusted, e.g. the pulse length, the time delay between two pulses, number of pulses measured etc. The evaluation is done externally with a Matlab program.

4.2 Contactless resistivity measurement method evaluation

On various CdTe samples measured with the COREMA measuring system, a change in the calculated resistivity is observed dependent on the change of the sweep time, meaning frequency of the pulses. As an example for this and further measurements a sample E50I1 was chosen. This sample is an undoped CdZnTe with 3.5% amount of zinc, grown at the Institute of Physics of Charles University in Prague. It was grown by the VGF method. The sample was taken from the center part of the ingot. At first a resistivity map with the sweep time of $20.48\mu s$ was measured as a further reference. Then three measuring points were selected and labeled dot1, dot2 and dot3 respectively, see **Fig. 13**.

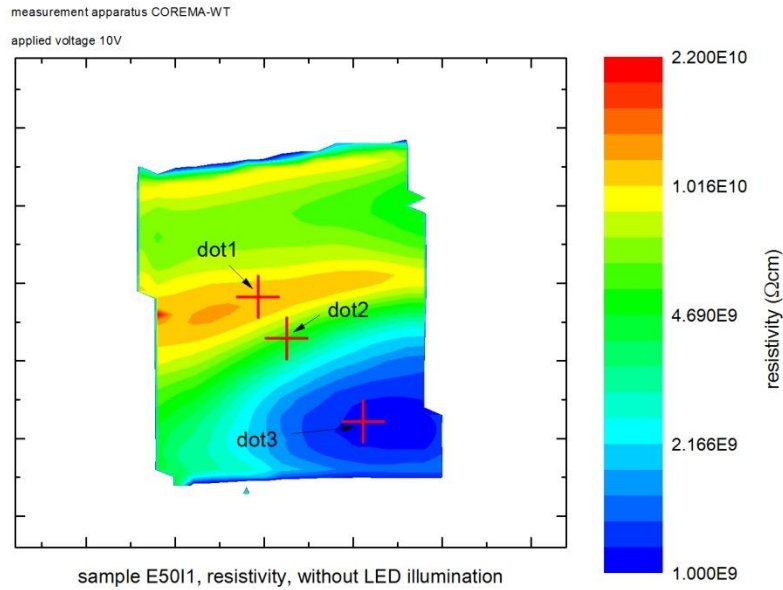


Fig. 13 Resistivity map of E5011 and the labeling of measurement points

In each of the points resistivity was measured with five different sweep times, the parameters were averaged from 64 measurements. The results for dot1 are shown in **Table 5**.

sweep time (μs)	frequency (Hz)	resistivity (Ωcm)	τ (μs)	Q_0 (abs.u.)	Q_{inf} (abs.u.)	σ^4 (abs.u.)
20.48	23.84	$8.20 \cdot 10^9$	$1.45 \cdot 10^4$	0.166	0.314	$9.56 \cdot 10^{-2}$
40.96	11.92	$1.08 \cdot 10^{10}$	$2.51 \cdot 10^4$	0.164	0.406	$4.89 \cdot 10^{-2}$
81.92	5.96	$1.33 \cdot 10^{10}$	$3.34 \cdot 10^4$	0.169	0.454	$6.02 \cdot 10^{-3}$
163.8	2.98	$1.39 \cdot 10^{10}$	$3.51 \cdot 10^4$	0.172	0.463	$1.16 \cdot 10^{-3}$
327.7	1.49	$1.44 \cdot 10^{10}$	$3.71 \cdot 10^4$	0.173	0.474	$2.23 \cdot 10^{-4}$

Table 5 Frequency dependence of E5011, dot1

We can see that the evaluated resistivity almost doubles with the decrease of the frequency of the pulses, as do τ and Q_{inf} . On the contrary, the value of the dielectric charge Q_0 remains relatively the same. With a lower frequency, the goodness of fit appears to be better. To explain this behavior we have developed a

⁴ Goodness of fit calculated by Corema-WT

theory of the charge carrier transport including the energy levels in the semiconductor.

First approach to the problem was to take the Shockley-Read recombination model with the assumption of one deep level localized on the surface and to calculate the dynamics of the free electrons at the surface and the electrons trapped at the deep level. The kinetic equations were

$$\begin{aligned}\frac{dn}{dt} &= -U_t + \sigma E \\ \frac{dn_t}{dt} &= U_t\end{aligned}\tag{52}$$

where U_t is the Shockley-Read recombination (9) without the generation parameter⁵. In this first approximation the conductivity is a constant. In the moment of measurement, the electron concentration varies a little from the equilibrium state and the following equation is valid

$$\begin{aligned}n &= n_0 + \Delta n \\ n_t &= n_{t0} + \Delta n_t\end{aligned}\tag{53}$$

If we apply this to (52) and calculate only for the concentration changes in the simplest approximation taking linearized form of U_t and assuming the electric field E to be consisting of the initial value E_0 and of a component that screens it, depending on the carrier concentration, with the parameter α

$$E = E_0 - \alpha(\Delta n + \Delta n_t)\tag{54}$$

we get the equation (here written in a matrix form)

$$\begin{aligned}\begin{pmatrix} \dot{\Delta n} \\ \dot{\Delta n}_t \end{pmatrix} &= \left(\gamma_e \begin{pmatrix} -N_t + n_{t0} & n_0 + n_1 \\ N_t - n_{t0} & -n_0 - n_1 \end{pmatrix} - \sigma\alpha \begin{pmatrix} 1 & 1 \\ 0 & 0 \end{pmatrix} \right) \cdot \begin{pmatrix} \Delta n \\ \Delta n_t \end{pmatrix} \\ &+ \begin{pmatrix} \sigma E_0 \\ 0 \end{pmatrix}\end{aligned}\tag{55}$$

The eigenvalues and eigenvectors to this equation without the constant part are

⁵ $U_t = \gamma_e((N_t - n_t) \cdot n - n_t n_1)$

$$\lambda_1 = -\sigma\alpha, \vec{U} = \begin{pmatrix} 1 \\ \frac{\gamma_e(N_t - n_{t0})}{\gamma_e(n_0 + n_1) - \sigma\alpha} \end{pmatrix} \quad (56)$$

$$\lambda_2 = -\gamma_e\beta, \vec{V} = \begin{pmatrix} 1 \\ -1 \end{pmatrix}$$

where $\beta = N_t - n_{t0} + n_0 + n_1$ and therefore the solution of the homogeneous equation reads

$$\Delta n = A e^{-\sigma\alpha t} + B e^{-\gamma_e\beta t}$$

$$\Delta n_t = A \frac{\gamma_e(N_t - n_{t0})}{\gamma_e(n_0 + n_1) - \sigma\alpha} e^{-\sigma\alpha t} - B e^{-\gamma_e\beta t} \quad (57)$$

This is equal to the state when the voltage isn't applied to the measurement circuit. But the mechanism for charging and discharging a capacitor should be the same. Now it is clear that if we calculate the charge carriers contributing to the measurement $\Delta q = \Delta n + \Delta n_t$, the exponential function with trapping rate and carrier concentration dependence falls out. Therefore only the electrons which are regrouping to screen the electrical field contribute to the measurement. As a conclusion of this theory, the assumption that the resistivity changes due to a deep level trapping and emitting charge carriers does not seem to be valid.

In the next model we take into account that the resistivity can be dependent on the electric field throughout the sample. From now on we calculate only the whole change of the charge carriers $\Delta q = \Delta n_t + \Delta n$ and assume local equilibrium between free and trapped electrons, i.e. fast charge exchange between trap and band. Because of Eq. (52) it is clear, that the change of charge carrier concentration in time is affected only by the electric field and conductivity, which we now develop to the first degree of Taylor's expansion.

$$\sigma(E) = \sigma(E)|_0 + \left. \frac{\partial \sigma}{\partial E} \right|_0 \cdot E = \sigma_0 + \sigma_1 E \quad (58)$$

This relation together with Eqs. (52) and (54) gives an equation for the charge carriers

$$\frac{d\Delta q}{dt} = \sigma_1 \alpha^2 (\Delta q)^2 - (2\sigma_1 \alpha E_0 + \sigma_0 \alpha) \Delta q + E_0 (\sigma_0 + \sigma_1 E_0) \quad (59)$$

First we calculate the roots of this quadratic function and the solution to the differential equation we get using partial fractions

$$\frac{1}{\alpha \sigma_0} \cdot \left(\frac{d\Delta q}{\Delta q - \frac{\sigma_1 E_0 + \sigma_0}{\sigma_1 \alpha}} - \frac{d\Delta q}{\Delta q - \frac{E_0}{\alpha}} \right) = dt \quad (60)$$

After integration of (60) and another editing, we get the temporal development of the charge carriers

$$\Delta q = \frac{E_0}{\alpha} + \frac{\sigma_0}{\alpha(\sigma_1 - C \cdot \exp(\alpha \sigma_0 t))} \quad (61)$$

Here the C is an integration constant that serves as a shift in time, so a singularity wouldn't be in the origin of time.

Determination of the origin also gives the start amount of free electrons. Therefore if we want the charge in the moment of the voltage application to be zero, we can simply subtract the same equation in $t = 0$. In the whole calculation we assumed only the charge that charges a capacitor, but in the case of dielectric material after voltage application, a polarization charge is established within picoseconds. The measurement time and sampling rate of the measuring instrument is higher than the time of polarization and therefore a polarization charge $\Delta q'_0$ (parallel to Q_0 in (43)) must be included in the equation. The final equation for the charge carriers in dependence on time is

$$\Delta q = \frac{\sigma_0}{\alpha(\sigma_1 - C \cdot \exp(\alpha \sigma_0 t))} - \frac{\sigma_0}{\alpha(\sigma_1 - C)} + \Delta q'_0 \quad (62)$$

To further understand the frequency dependence of resistivity the samples were measured at FMF Freiburg, where the frequency step between measurements can be better adjusted and asymmetrical pulses can be applied. The measured samples were E50I1 from Prague and two standard commercial CdTe:Cl detector-grade Acrorad samples, marked ARSP-2 and ARSP-3.

sample	material	doping	resistivity (Ωcm)	manufacturer
ARSP-2	CdTe	Cl	$\sim 2 \cdot 10^9$	Acrorad Co.Ltd.
ARSP-3	CdTe	Cl	$\sim 5 \cdot 10^9$	Acrorad Co.Ltd.
E50I1	$\text{Cd}_{0.965}\text{Zn}_{0.035}\text{Te}$	none	$\sim 3 \cdot 10^9$	MFF UK ⁶

Table 6 *Samples used for resistivity, time delay and frequency dependency measurement*

At first the resistivity was mapped on all the samples just to determine the spatial distribution and to decide if only one representative point measurement can be measured on the sample or if the resistivity varies too much and more point measurements must be done to fully evaluate the behavior of the sample. The resistivity distribution was already measured on the E50I1 sample in Prague, so the same measurement points were set, see **Fig. 13**. As seen on **Fig. 14**, the Acrorad samples have a good homogeneity of the resistivity, so one measurement point was set in the middle of the topograms.

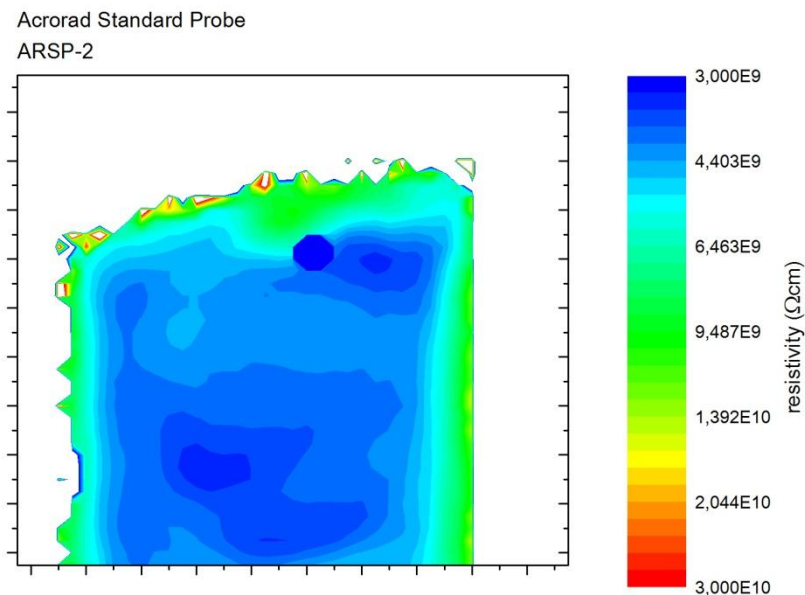


Fig. 14 *Resistivity map of ARSP-2*

⁶ Sample was grown at Technical laboratory of Institute of Physics of Charles University, Prague

4.3 Resistivity dependence on time delay between pulses

In order to understand the details of charge transport asymmetric pulses were applied to the sample with the on time of $T_{HIGH} = 0.013s$ and the time T_{LOW} , where no voltage is applied, was altered. In every measurement the bias pulses of 10 volts were used and 1000 pulses were measured and averaged to decrease inaccuracy of the measurement instruments. All the parameters were evaluated using Eq. (50) with a Matlab program. As a representative the Acrorad Sample ARSP-2 was chosen. The summary of other samples is shown in Table 7.

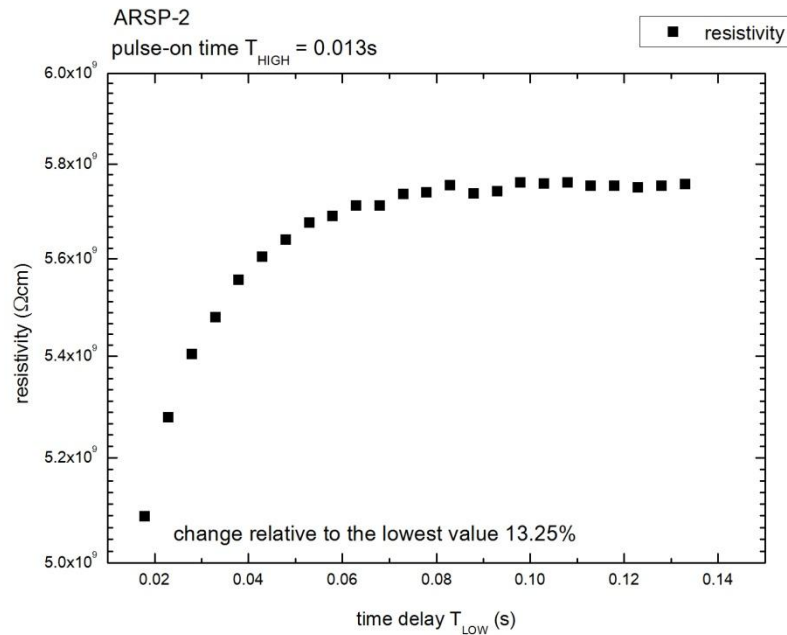


Fig. 15 Resistivity dependence on time delay between the pulses on the sample ARSP-2

From Fig. 15 we can see that the resistivity seems to increase with a higher time delay between the applied pulses. The relative change in the resistivity related to the lowest value is about 13%. But if we check the same dependence of all the measured parameters on Fig. 16, Fig. 17 and Fig. 18, we can see that the charge Q_0 almost doubles in the measurement, Q_{inf} increases by more than half and τ has a descending trend with a longer pulse delay. According to the theory presented above,

the initial charge should be constant and not dependent on the pulse length. This phenomenon will be discussed below.

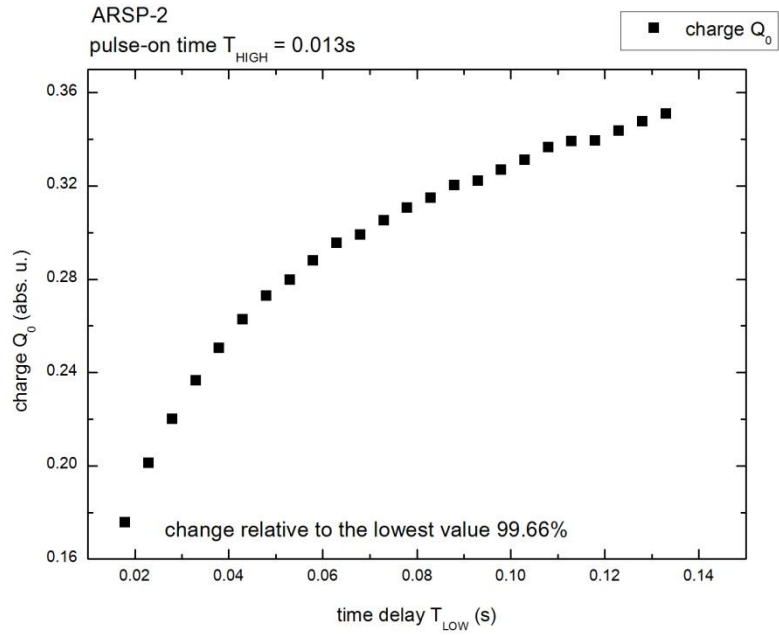


Fig. 16 *Initial charge dependence on the time delay between pulses*

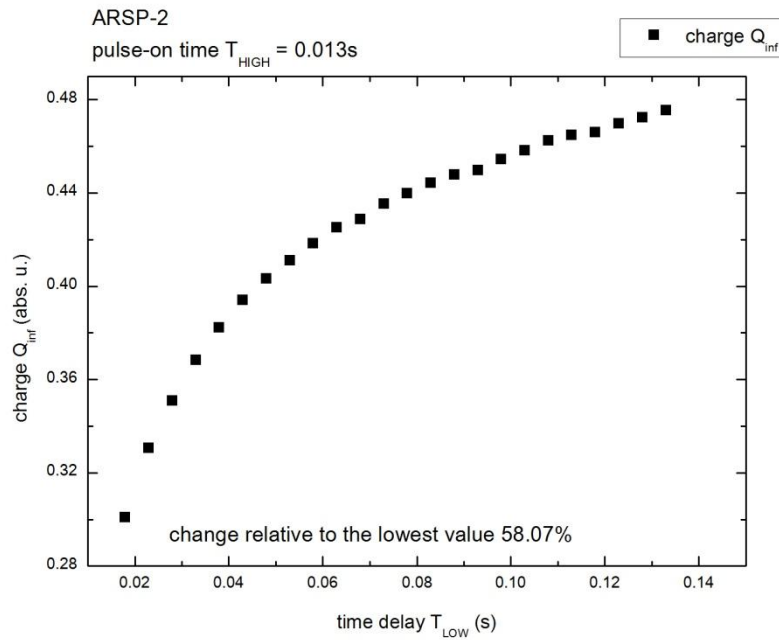


Fig. 17 *Charge Q_{inf} dependence on the time delay between pulses*

As Eq. (38) shows, τ is the parameter that is bound to the resistivity we want to evaluate. Now it's clear that the change in resistivity is caused by the behavior of the evaluated charge parameters and has an inverted dependence to the parameter τ , to which it should correlate.

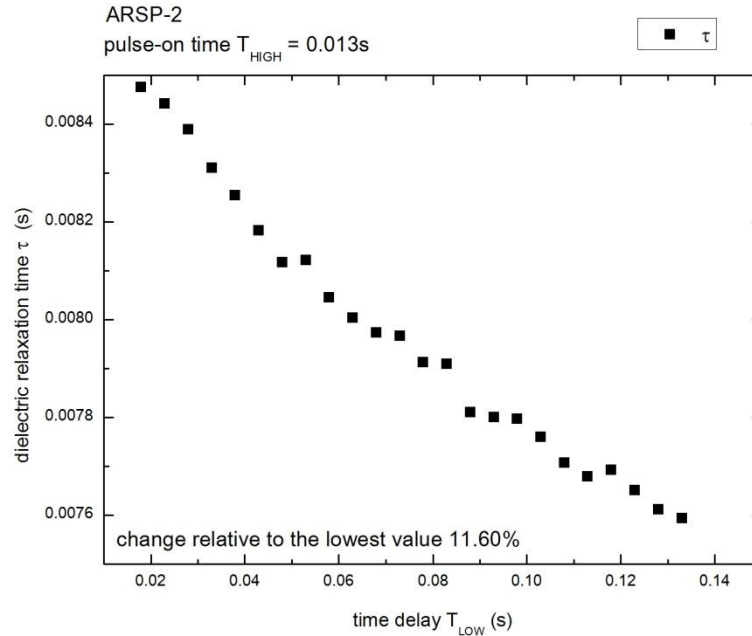


Fig. 18 *Relaxation constant τ in dependence on the time delay between pulses*

The change in the initial charge is included in Eq. (61) in the parameter C . It is probable that in the first applied pulse the charge is transported within the sample and when the voltage is turned off, the charge tries to go back to reach an equilibrium. If the turn-off time is too short, the charge does not manage to return to the starting state. Then in the next voltage pulse this charge is already present and the initial charge is not only the polarization charge, as described in (62).

But the assumption is that this charge is insignificant compared to the $\Delta q'_0$. By increasing the delay between the pulses, the charge has more time to relax and therefore the measured charge Q_0 should decrease with the increased T_{LOW} or not change at all. To support this statement we can look at the measurement with Corema-WT shown in **Table 5**, where we can see that the initial charge varies very little. Therefore the change in the Q_0 in measurement in Freiburg is attributed to the

scanner and charge amplifier characteristics and from now on we discuss only the parameters τ and Q_{inf} .

sample	tendency of				change relative to the lowest value			
	ρ	Q_0	Q_{inf}	τ	ρ (%)	Q_0 (%)	Q_{inf} (%)	τ (%)
ARSP-2	I	I	I	D/S	13.25	99.66	58.07	6.01
ARSP-3	I	I	I	D	15.08	100.22	58.08	10.0
E50I1, dot1	I	I	I	I	15.78	54.54	57.89	20.92
E50I1, dot2	I	I	I	D/S	7.91	57.52	36.86	9.99
E50I1, dot3	I	I	I	D/S	43.70	124.07	52.11	2.96

Table 7 *Dependencies and relative changes of measured parameters on all used samples; I-increasing, D-decreasing, S-partially stagnating*

We apply the equation (62) to the interface of the sample and the air gap, where the measurement actually occurs. The parameter σ_1 depends on the band bending. There are four possibilities depending on the conductivity type of the sample and the sign of σ_1 . First two choices are an n-type material with bands curved downwards and a p-type with bands curved upwards. This would mean that the surface is more conductive than the bulk and the charge would be faster dispersed on the surface. With the guard ring around the scanner this would produce a perfect resistivity measurement with this method and no frequency dependence effect could be visible. Other two choices are a p-type with bands curved downwards and an n-type upwards. Now we move to the representation, where throughout the measurement of one period (the time of pulse on and off) an average electrical field of

$$E_{AV} = \frac{E_{ON} \cdot T_{HIGH} + E_{OFF} \cdot T_{LOW}}{T_{HIGH} + T_{LOW}} \quad (63)$$

lies on the sample. It means that with a longer time delay the average field decreases. We assume that the bulk majority charge is measured.

The results can be explained using a changing barrier on the surface. With longer pulses, i.e. decreased average field, the resistivity decreases. That means the barrier must be smaller with a lower average electric field. The scanner applies a

negative voltage to the sample in our scheme and therefore we choose to investigate the n-type with bands curved upwards.

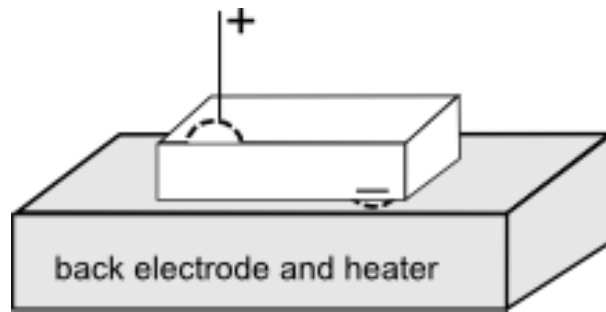


Fig. 19 Arrangement of the Seebeck effect measurement

This choice is supported with a measurement of thermoelectric effect, shown in **Fig. 19** and **Fig. 20**. In this measurement we observed decrease in the magnitude of negative electrical current when the cathode was heated. This result corresponds to the situation when electrons are transported in temperature gradient to the upper contact (cathode) and screen the positive charge there. Therefore the conductivity of the sample is of n-type.

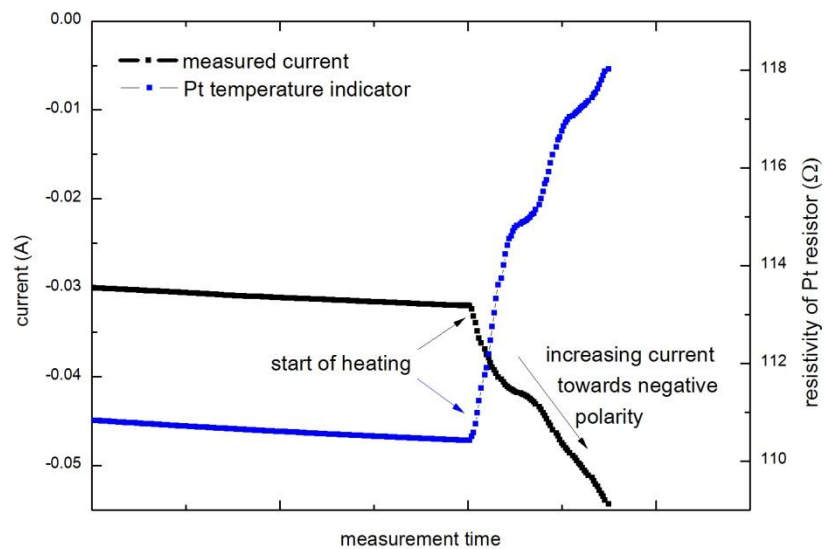


Fig. 20 Measured Seebeck effect of the sample ARSP-2

Now we investigate what happens with the band structure in the time delay measurement. With no voltage applied the bands are bent upwards and the sample is in an equilibrium state, as shown in **Fig. 21**.

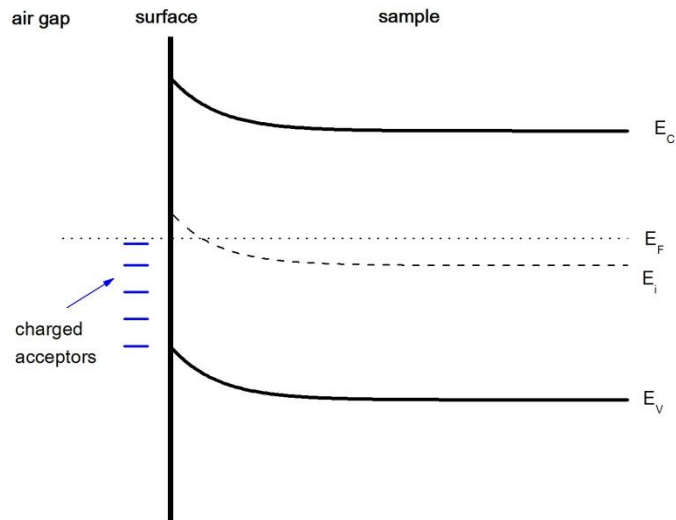


Fig. 21 *The band structure in equilibrium state, before the measurement, $t=0s$*

The curvature of the bands is given by the charged acceptors on the surface of the sample. When the voltage is applied, the Fermi level turns to an electrochemical potential and the band structure tilts (**Fig. 22**). Electrons are pulled away from the surface, whereas holes, which begin to screen the potential, are attracted to it.

The total voltage on electrodes must remain the same through the whole measurement and the slope of the potential in the sample decreases due to charging of the surface layer and screening of the electrical field. Simultaneously, the slope of the potential on the air gap must increase. The application of the voltage entails that the electrons are pushed away from the surface and the Fermi level shifts towards the valence band and so less acceptors on the surface are charged⁷ as shown in **Fig. 23**.

⁷ The Fermi level shifts and more holes drift to the surface and there they discharge acceptors.

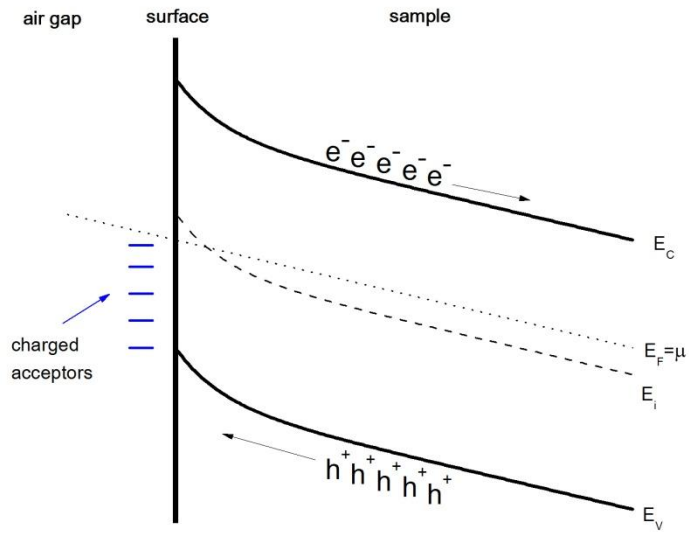


Fig. 22 *The tilted band structure immediately after application of the electric field, $t \approx 10ps$*

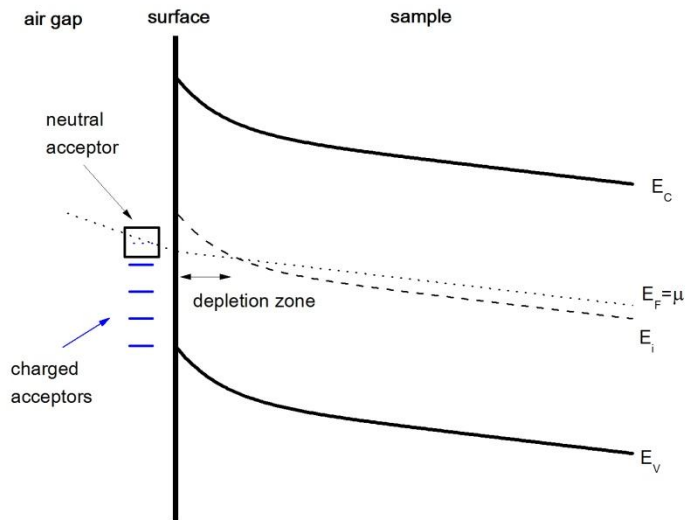


Fig. 23 *Straightening of the band structure, shielding the potential on the air gap, $t \approx 1ms$*

Even with less surface charged acceptors the band bending increases because of relatively higher potential on the air gap, which repels electrons and results in an extension of positively charged region in the bulk.

Finally, in the limit of infinite time the band structure becomes almost as in the initial state with an exception of lower Fermi energy at the surface and larger band bending so that the Fermi energy tends to the equilibrium farther in the bulk, see **Fig. 24**.

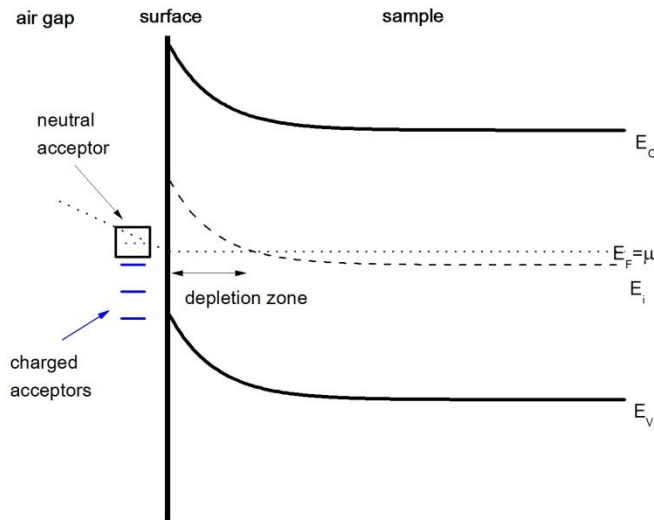


Fig. 24 *The band structure in the infinite time, $t \approx \infty$*

Now we can see that the application of the electric field actually bends the bands and tilts the whole band structure, so that the electrons must overcome a higher barrier to get to the surface. Thus fewer electrons get to be measured by the sensor. If the time delay between the pulses is higher (meaning the average voltage is lower) the surface barrier becomes effectively lower and more electrons may contribute to the conductivity measured.

This means that with a lower average voltage applied a higher conductivity (lower resistivity) is measured, which is consistent with the measurement shown in **Fig. 18** and **Table 7**.

4.4 Resistivity dependence on frequency

On all of the samples a frequency dependency with symmetric pulses was also studied and is representatively shown on the sample ARSP-2. The tendencies

and relative changes in the parameters of the other samples are shown in **Table 8**. Unfortunately same frequencies as studied in Prague could not be measured in Freiburg because of the apparatus setup and parameters; however the range of 25-100Hz could be investigated in smaller steps.

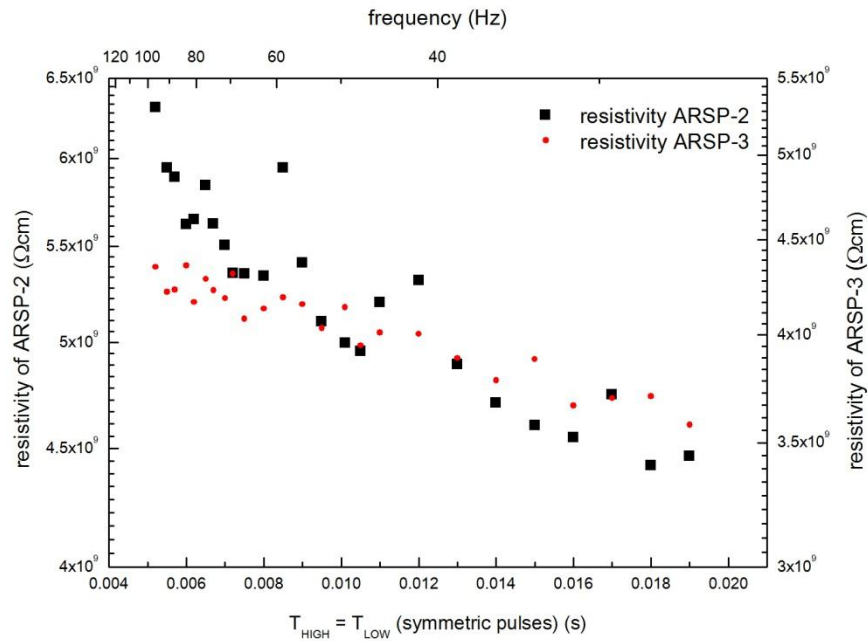


Fig. 25 *Frequency dependence of resistivity on sample ARSP-2*

In **Fig. 25** we can see that the resistivity decreases with a prolonged time delay between the pulses. But now not only this delay varies, but also time T_{HIGH} , when the pulse is applied to the sample. The decreased resistivity with lower frequency seems to be in contradiction with the previous measurement (time delay between the pulses dependence). Also some points, which do not follow the general tendency can be seen. If we look closer **Fig. 25** seems to have resonance peaks at the frequencies 20Hz, 40Hz, 60Hz and 80Hz, which will be looked at closer below. To better understand the behavior in this experimental setup, the individual parameters must be examined, as above.

sample	tendency of				change relative to the lowest value			
	ρ	Q_0	Q_{inf}	τ	ρ (%)	Q_0 (%)	Q_{inf} (%)	τ (%)
ARSP-2	D	D	S	S	42.64	20.15	3.43	18.35
ARSP-3	D	D	I/S	I	21.80	22.79	3.44	14.08
E50I1, dot1	I/S	D/S	I	I	68.11	15.96	96.31	409.39
E50I1, dot2	D	D	S	I/S	70.96	61.38	2.50	12.12
E50I1, dot3	D	D	S	I/S	45.54	53.72	5.87	13.05

Table 8 *Tendencies and relative changes of parameters; I-increasing, D-decreasing, S-partially stagnating*

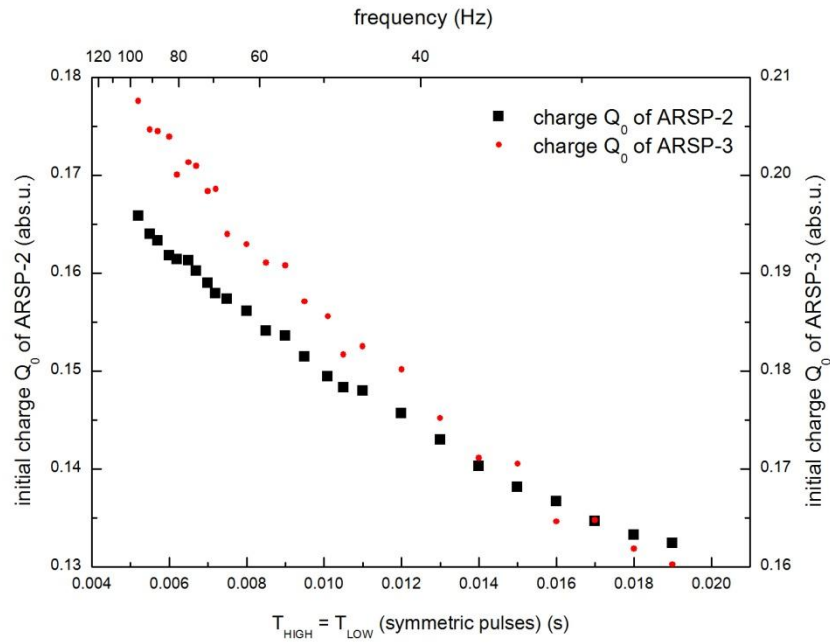


Fig. 26 *Frequency dependence of the charge Q_0 on sample ARSP-2*

As we can see on **Fig. 26** the initial charge has a decreasing tendency with longer pulses and off-time between them. The tendency is inversed compared to the results from the time delay between pulses measurement. However, in the interpretation we must be careful, because the experiment setup is different. From **Fig. 26**, **Fig. 27** and from **Table 8** we can see that the change in the initial charge Q_0 relative to the lowest value is about 20 percent. The infinite charge however varies only about 3 percent. This supports our claim mentioned above that the measured change in Q_0 is

contributed to the characteristics of the charge-sensitive amplifier and further signal adjustment. The measured value of Q_{inf} can be affected with this, but we do not assume this⁸.

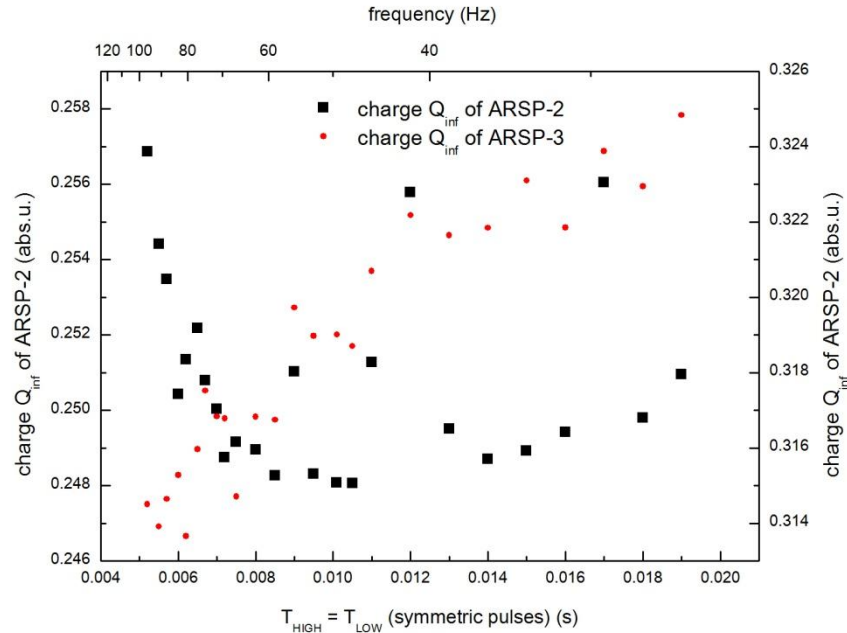


Fig. 27 Frequency dependence of the charge Q_{inf} on sample ARSP-2

Now we can assume Q_{inf} to be almost constant. If we look at **Fig. 28**, we can see that in the dependence of the dielectric constant τ there seem to be some resonance peaks, which correspond to the offset points in **Fig. 25**. The same points are visible in **Fig. 27**. The resonance at the frequencies of n-times 20Hz is not likely attributed to some response of the sample. Therefore they seem to be some artifacts of the measuring apparatus and should be excluded from the parameter evaluation. They were not visible on measurements of all the samples.

For comparison results of the sample ARSP-3 are shown in the **Fig. 25** and **Fig. 28**.

⁸ The assumption is that the value of the charge measured long after the start of the measurement is almost not influenced by the response function of the charge sensitive amplifier. The measured value can have a systematic error, which is neglected here.

Now we evaluate the tendencies of the measured parameters. The decrease of Q_0 is contributed to the characteristics of the charge-sensitive amplifier, Q_{inf} and τ seem to be constant. If we try to explain this experiment with the approach used above, we now have an average field that is constant throughout the whole measurement, because we use symmetrical pulses, so the field is on the same amount of time as it is off in all the measurements. With this fact, we see that using our theory of the tilting of bands as a result of the average field application, the resistivity, Q_{inf} and τ should be constant.

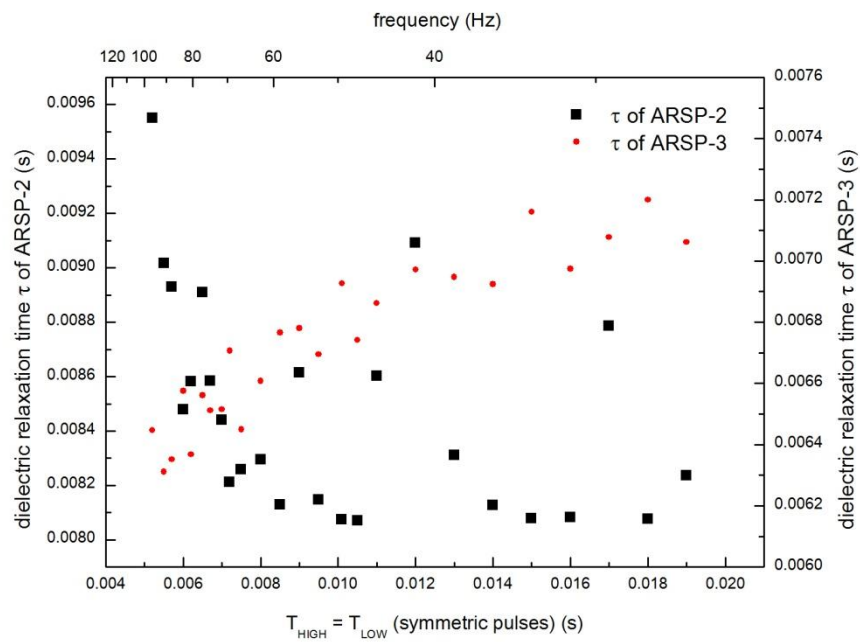


Fig. 28 *Frequency dependence of the relaxation time τ on sample ARSP-2*

Now if we look at **Table 5** and **Table 8**, we see that with lower frequency the relaxation time τ increases and so does the ultimate charge. The behavior of both parameters is similar in both measurements, but on the TDCM in Freiburg other range of frequencies was measured.

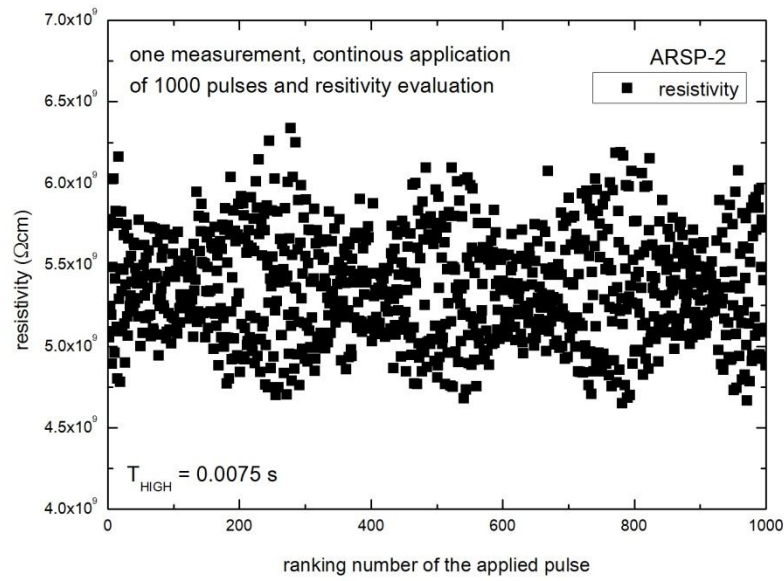


Fig. 29 *Inaccuracy of the measurement due to resonance of the measuring circuit*

If we take a look at the behavior of the relaxation constant measured on COREMA, we see that with lower frequencies the parameter value increases. This seems to be in contradiction with the results of the time delay dependence measurement. Here we must be cautious because here not only the time between the pulses changes, but also the on-time of the pulse. On (62) we can see that the relaxation process is a function, which varies slightly from an exponential function. In both measurement sets we actually study other parts of the process. In **Fig. 30** we can see a scheme of what parts of the relaxation process is actually measured.

In the time delay study the pulse-on time remains constant, the whole measurement corresponds to the first part of the function. Only fast processes can be measured here. But in the frequency dependence investigation, we prolong the measurement time and thus slower processes, such as trapping at slow trap or recombination center, can contribute to the result and effectively increase the relaxation constant τ .

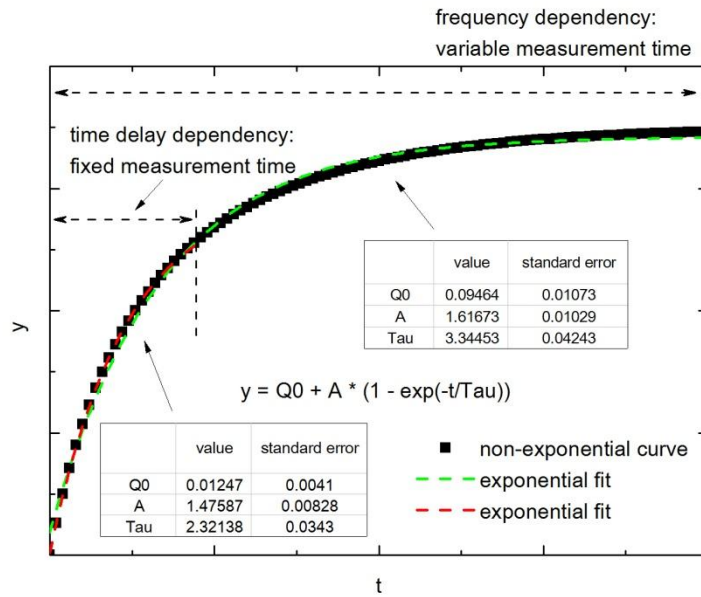


Fig. 30 *Example of non-exponential charge transport behavior and influence of the length of the measurement on the parameter evaluation*

For the practical utilization of features discussed above, we should disclose the proximity of determined data to the real bulk resistivity of the measured samples.

Based on the theory introduced above, we may summarize that the deviations of the resistivity are due to band bending, which depletes the surface layer and increases the resistivity in that region. The variations at the resistivity may be thus used as the simplest test of the effect of band bending to the evaluated resistivity. Simultaneously, the lower band bending reached by longer T_{LOW} in the first case or by high frequency in the second case assures resistivity more closely to the right value. Nevertheless, as an exact band bending cannot be determined in these experiments, the real bulk resistivity may be only guessed as lower than the minimum value found in reported measurements.

The decreased resistivity with lower frequency measured with the TDCM method in Freiburg is assessed as the effect of the change in the initial charge. However the tendencies of parameters Q_{inf} and τ are in agreement with the presented theory.

4.5 Resistivity and photoconductivity

The possible correlation between resistivity and photoconductivity has been studied using the modified Corema-WT apparatus described in Ref. [13]. The purpose of the investigation was to first of all localize areas of lower photoconductivity, which should correspond to areas with increased concentrations of recombination centers. The second purpose was to look whether the distribution of photoconductivity is in some relation to other physical properties (resistivity, photoluminescence) and to the growth conditions.

sample	material	doping	resistivity (Ωcm)	manufacturer
Madrid 1 ⁹	$\text{Cd}_{0.9}\text{Zn}_{0.1}\text{Te}$	In (5-10 ppm)	$\sim 4 \cdot 10^9$	Madrid University ¹⁰
Madrid 2 ¹¹	$\text{Cd}_{0.9}\text{Zn}_{0.1}\text{Te}$	In (5-10 ppm)	$\sim 3 \cdot 10^9$	Madrid University ¹⁰
E50I1	$\text{Cd}_{0.965}\text{Zn}_{0.035}\text{Te}$	none	$\sim 3 \cdot 10^9$	MFF UK ¹²
E50I2	$\text{Cd}_{0.965}\text{Zn}_{0.035}\text{Te}$	none	$\sim 1 \cdot 10^9$	MFF UK ¹²

Table 9 *Samples used for resistivity, photoconductivity and deep level spectroscopy measurement*

The samples used in this measurement were E50I1 and E50I2. Furthermore two CdZnTe samples grown at the University of Madrid were investigated (labeled Madrid1 and Madrid2). These samples were grown using the VGF method, each one was grown with a different temperature gradient setting. Detailed description of the growth method, the set of growth parameters and Figs of the crystals are shown in our Ref. [24]. For the purposes of our investigation the fact was important, that in the growth of the first ingot the temperature gradient was constant whereas with the second ingot the gradient was adjusted during the growth phase. The samples were harvested from the middle section of the ingot along the axial direction.

⁹ Further referred as sample No.1

¹⁰ Crystal Growth Laboratory of Universidad Autonoma de Madrid

¹¹ Further referred as sample No.2

¹² Sample was grown at the Technical laboratory of the Institute of Physics of Charles University, Prague

The resistivity and photoconductivity investigation was done with the autotune setting on the measurement device. This means that after measuring one pulse, the sweep time (see above) is automatically set to the one that has the best goodness of fit parameter.

First of all the resistivity maps were measured.

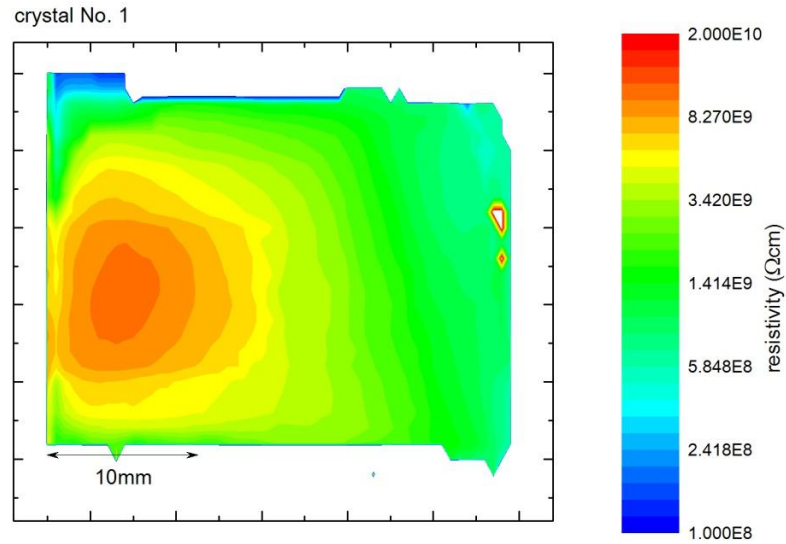


Fig. 31 *Resistivity map of crystal No. 1*

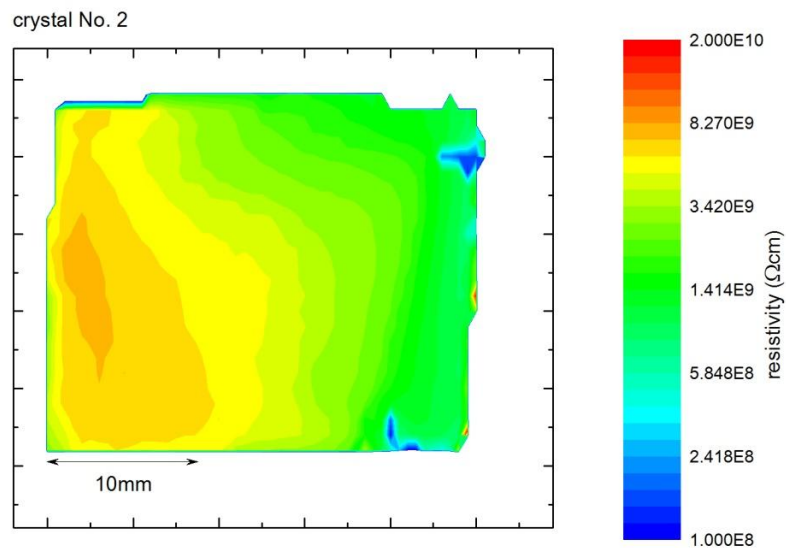


Fig. 32 *Resistivity map of crystal No. 2*

From the **Fig. 31** and **Fig. 32** we can see that both crystals have a maximum of resistivity located near the beginning of the sample, meaning close to the middle of the grown crystal. However, in the second sample, where the temperature gradient was adjusted, the region of high resistivity seems to be spread on a larger region of the crystal. This means that more of the ingot can be potentially usable as a radiation detector, if other important parameters, like the mobility-lifetime product, also fulfill the requirements on detector-grade crystals.

The charge collection efficiency is a parameter that quantifies the ability of a material to be used as a detector. This can be characterized with the lifetime-mobility product of electrons Ref. [24]. The modified Hecht relation (Ref. [25]) connects photoconductivity and the lifetime-mobility product. As described in Ref. [26], [27] the charge collection efficiency distribution can be predicted by mapping of the photocurrent.

In **Fig. 33** and **Fig. 34** photoconductivity map of the samples is shown. The LEDs with the maximum peak intensity at 830nm were used as the illumination source, see **Table 2**.

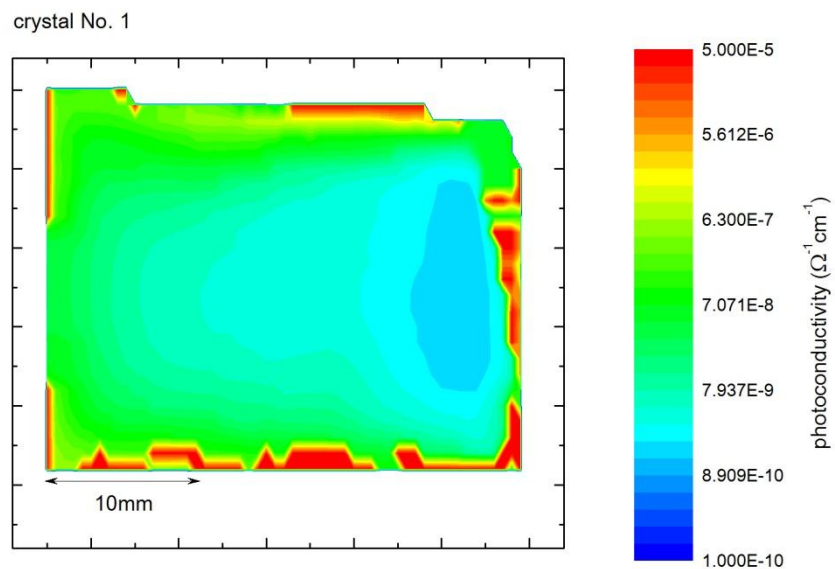


Fig. 33 *Photoconductivity map (with LED 830nm) of crystal No. 1*

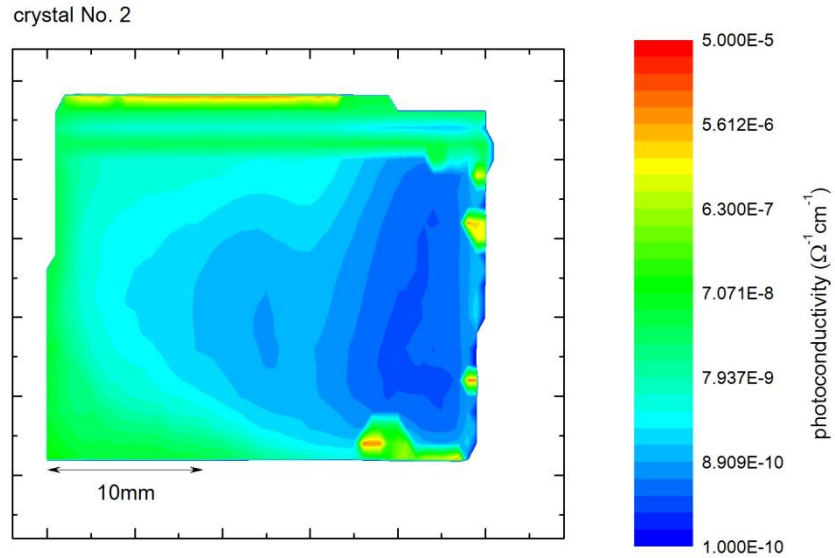


Fig. 34 Photoconductivity map (with LED 830nm) of crystal No. 2

We can see that the first sample has a small region of decreased photoconductivity at the end. The sample No. 2 has generally lower values of photoconductivity.

To highlight the differences between the two samples, line profiles along the growth axis were made.

In **Fig. 35** we can see that in the first sample resistivity reaches a maximum and further from the sample edge the resistivity decreases relatively rapidly. The sample No.2 has a lower resistivity maximum, but the further decrease is up to a certain point smaller than in the first sample. So, the resistivity appears to be more homogeneous in a larger region of the sample. Towards the end resistivity of both samples falls rapidly.

The difference in the maximal value of resistivity between the two samples can be explained by different Zn and In concentration in each sample.

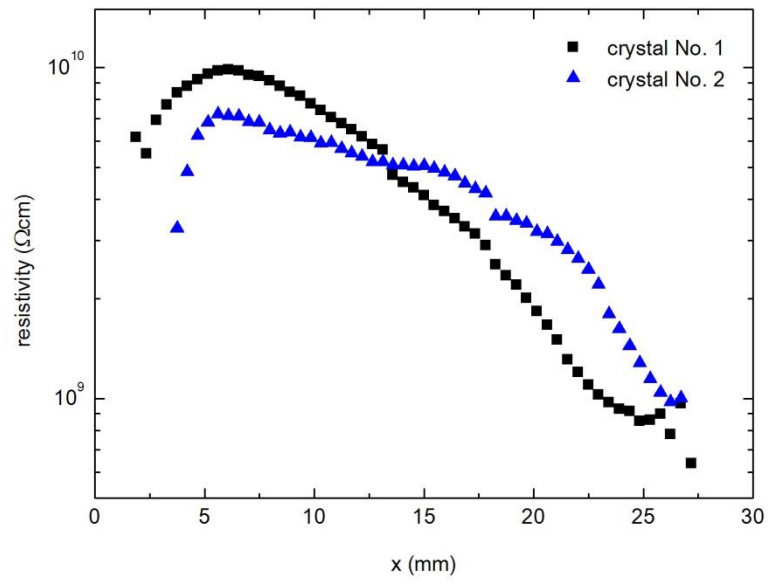


Fig. 35 *Resistivity profiles of both crystals, through the middle of the sample in the growth axis*

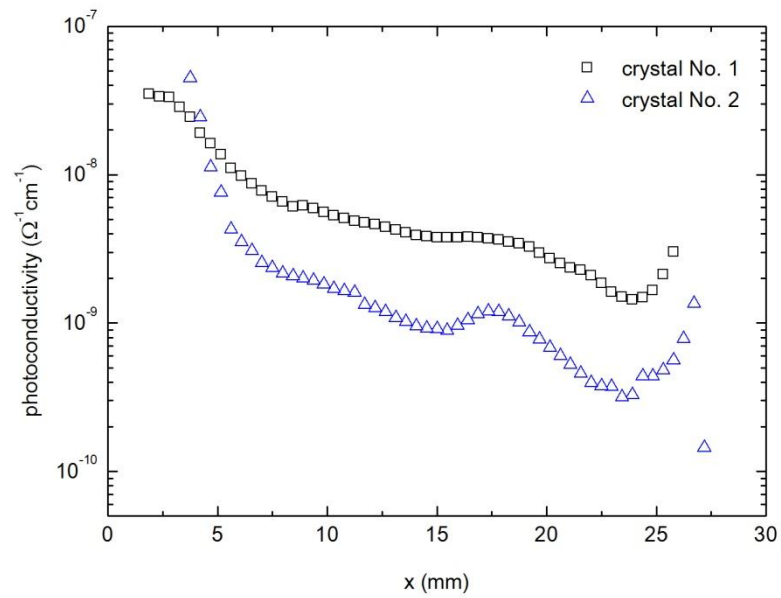


Fig. 36 *Photoconductivity profiles of both crystals, through the middle of the sample in the growth axis*

Photoconductivity profiles of both samples have a falling tendency. On the edges, the photoconductivity seems to rise. But as discussed in Ref. [13], the photoconductivity mapping¹³ on the edges of samples can have a greater measurement error. This is because of the reflection of the radiation on the apparatus electrodes and scattering on the sample's edge. Therefore these few millimeters of the edge should be excluded from the evaluation. Photoconductivity of sample No. 2 seems to have a local maximum just in front of the point, where resistivity has a turn and starts to fall rapidly. Connection between resistivity and photoconductivity for both samples is better displayed on Fig. 37 and Fig. 38, respectively.

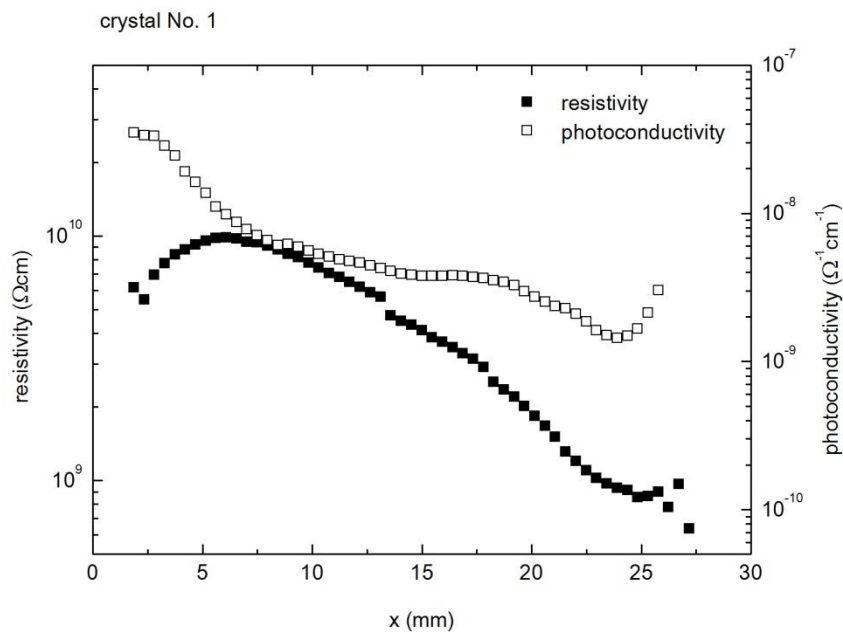


Fig. 37 *Profile of the resistivity and photoconductivity in crystal No. 1*

On sample No.1, in the first section the resistivity increases to its maximum and photoconductivity is declining throughout the whole sample, with a small stagnating phase. The parameters are therefore anti-correlated in the beginning. After the resistivity starts to decrease both measured variables correlate till the end of the sample.

¹³ In the setup described above

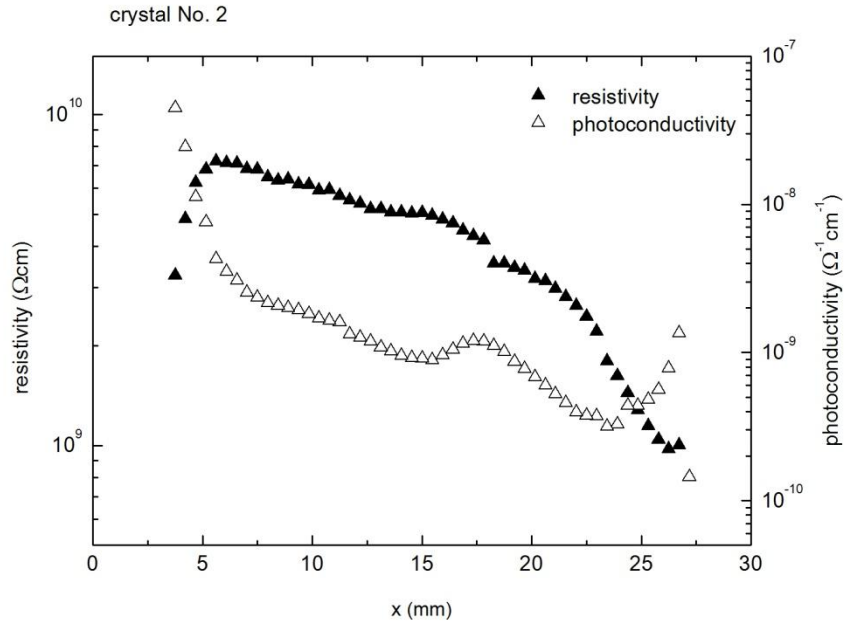


Fig. 38 *Profile of the resistivity and photoconductivity in crystal No. 2*

In the second sample resistivity has its maximum almost directly at the beginning and then it is slowly decreasing. The photoconductivity decreases through the sample. It has a small local maximum, but then starts to fall again. The values are systematically lower than in the first sample. But as in the sample No. 1 at first the parameters seem to anti-correlate in the region before the resistivity maximum. After that towards the end they are in correlation with a small anti-correlation phase, because of the local maximum of photoconductivity.

This behavior can be explained with a model where the resistivity change is due to change of the Fermi level. This model was proposed in Ref. [28], [29].

Occupation of some deep level close to the middle of the band gap can change if the Fermi level shifts. This will influence the trapping/re-trapping rates of this level and thus also the electrical and photoelectric properties of the material. Both the anti-correlation and correlation section can be described using this model.

The mechanism can be illustrated with an n-type sample with deep level and the Fermi level change towards the valence band, see **Fig. 39**. By lowering the E_F the electron occupation of the deep level decreases and the resistivity increases because of the compensation effect described above (**Fig. 39a**).

The maximal resistivity is achieved when the Fermi level coincides with the deep level (**Fig. 39b**) (the position of the deep level is assumed in the middle of the gap). With the decrease of the electron population of the deep level its trapping and recombination rates increases. This lowers the photoconductivity.

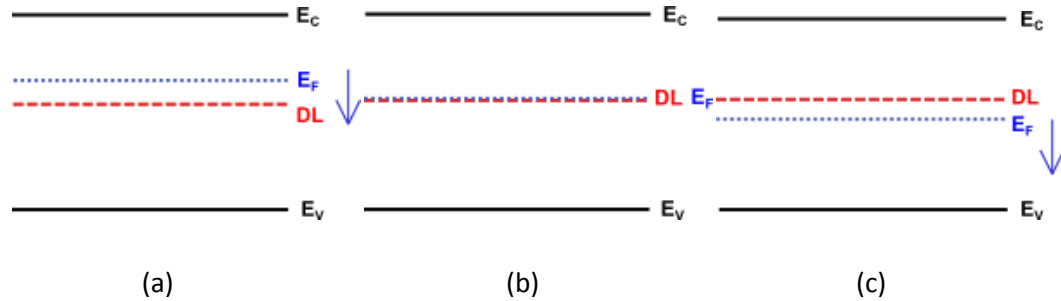


Fig. 39 *Scheme of the theory of the Fermi level shift*

As the Fermi level shifts further relative to the deep level, the resistivity and photoconductivity decrease (**Fig. 39c**). In this phase both parameters correlate. This means that the conductivity type changes near the point where the resistivity passes through the maximum. However the type of conductivity was not measured. It is assumed to be an n-type here because of the substantially higher electron mobility in CdTe and CdZnTe.

This mechanism and behavior was described in Ref. [26], but only anti-correlation of resistivity and photoconductivity was measured on the CdZnTe:In crystal. In the current work a transition between anti-correlation and correlation near the theoretical maximum can be observed. This can represent an argument for the validity of the proposed theory.

To furthermore support the presented theory of the Fermi energy shift photoluminescence spectra of the second crystal were measured. The experiment was conducted under the temperature of 4.2K and it was done by the measurement setup described above. The spectra measured at the beginning and at the end of the sample are presented in **Fig. 40**.

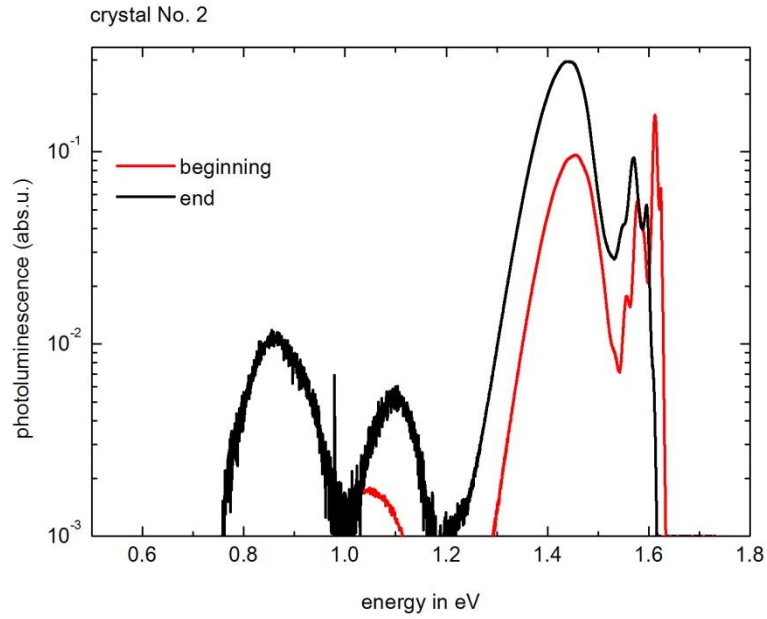


Fig. 40 *Photoluminescence of crystal No.2*

Focused on the midgap level (around 0.85eV) we can see that towards the end of the sample the photoluminescence increases. This may reflect also a change in the level occupation, caused by the Fermi energy shift. When the deep level empties itself, the radiant transitions with the conduction band become more frequent. This increases the intensity of the measured photoluminescence.

The measurement therefore supports the idea that a change of the equilibrium occupancy of a midgap level is a key factor limiting the charge collection efficiency.

4.6 Resistivity, photoconductivity and deep level spectroscopy correlation

As shown above, study of deep level luminescence together with resistivity and photoconductivity can be a powerful tool to characterize the material. To increase our understanding of recombination processes in CdTe and CdZnTe photoluminescence¹⁴, resistivity and photoconductivity of samples E50I1 and E50I2 were measured. The crystal E50I2 was chosen as a representative, the summary of evaluation of the sample E50I1 is shown in **Fig. 50**.

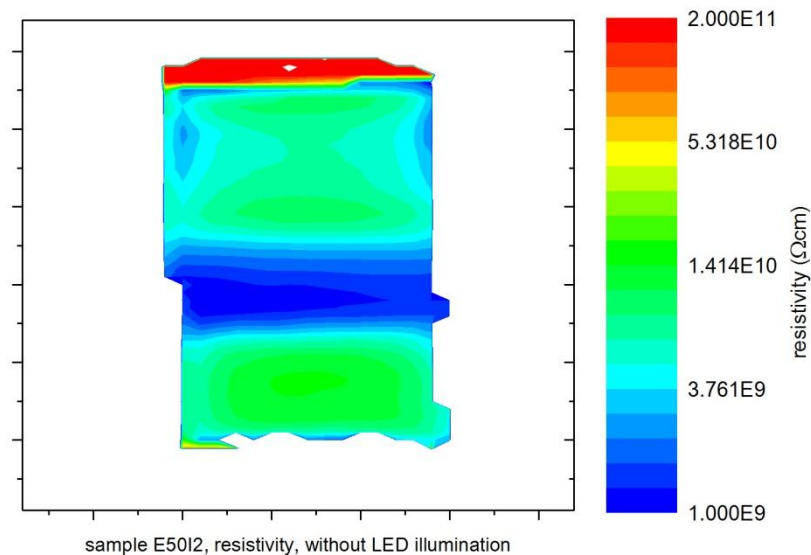


Fig. 41 *Resistivity map of sample E50I2*

On **Fig. 41** and **Fig. 42b** we can see that the photoconductivity with the source LED 1720nm is in anti-correlation with the resistivity in the central part of the sample. Edge effects can influence the photoconductivity results. Therefore values near the edges of the samples may not be correct.

¹⁴ PL - photoluminescence

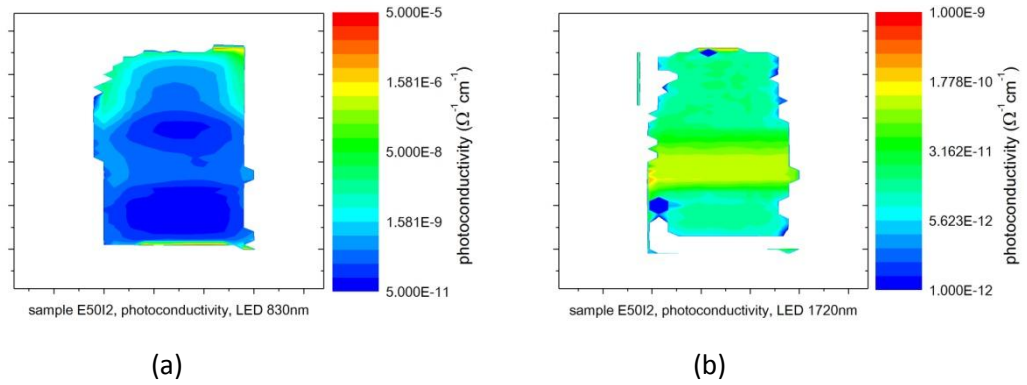


Fig. 42 Photoconductivity map of E50I2 with the illumination source
 (a) LED 830nm, (b) LED 1720nm

To better the understanding of the connection between resistivity and photoconductivity, a vertical profile in the middle of the sample was made.

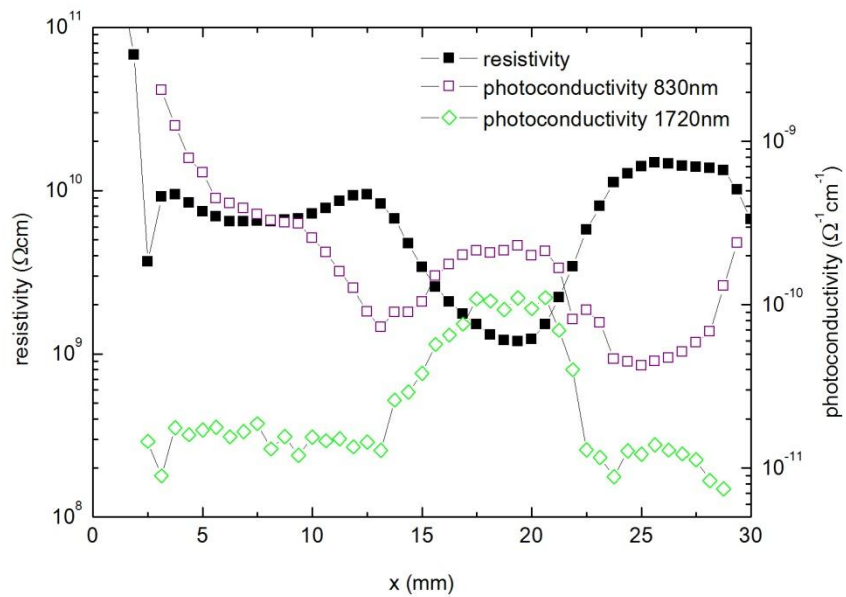


Fig. 43 Resistivity and photoconductivity profile of E50I2

In **Fig. 43** we can see that the photoconductivity (830nm) indeed has a good anti-correlation to the resistivity. The mean wavelength of the LED 1720nm is equal to 0.721eV mean energy of the photon incoming on the sample. This is very near the

midgap energy and therefore the signal can reflect the concentration of deep levels present in the material.

The deep level photoluminescence on the sample E50I2 was measured using the germanium detector, on the other sample (E50I1), InSb detector was used.

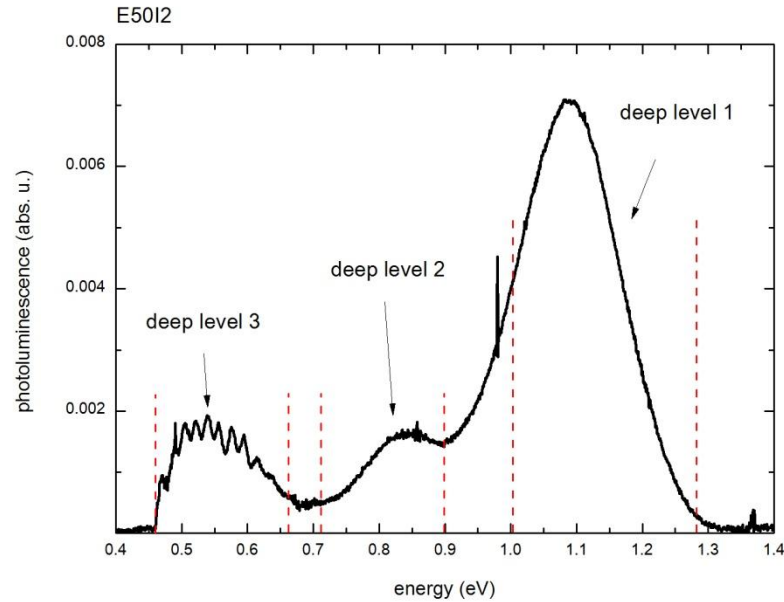


Fig. 44 *Photoluminescence measurement of one point of sample E50I2 using the He-Ne excitation laser and Ge detector*

Fig. 44 shows one photoluminescence measurement of the sample E50I2. From such measurement the range of significant peaks was determined. Within this range the peak was integrated and the value of the integral used as a photoluminescence parameter of this peak and the connected deep level. In the measurement of both samples, three deep levels were significant, see **Table 10**.

The oscillations observed on the $0.5-0.6\text{eV}$ are due to the used filter.

sample	deep level 1	deep level 2	deep level 3
E50I2	10300-8400cm ⁻¹ = 1.28-1.04eV	7250-5700cm ⁻¹ = 0.90-0.71eV	5300-3700cm ⁻¹ = 0.66-0.46eV
E50I1	10000-7500cm ⁻¹ = 1.24-0.93eV	7200-5650cm ⁻¹ = 0.89-0.70eV	5500-3400cm ⁻¹ = 0.68-0.42eV

Table 10 *Deep levels observed in the photoluminescence measurement*

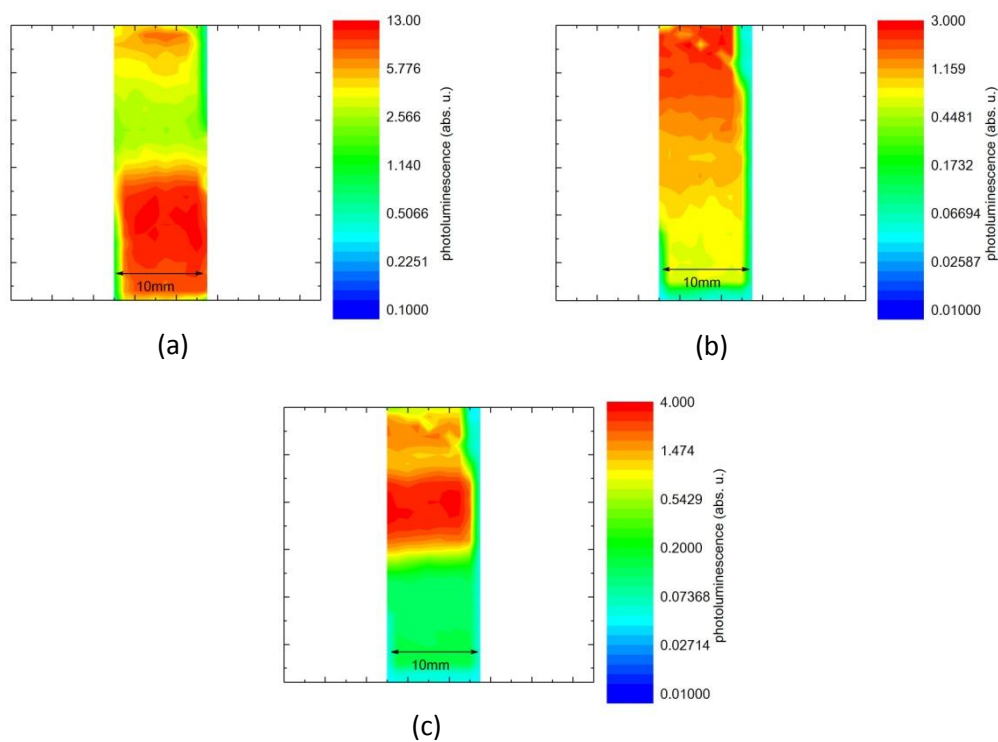


Fig. 45 *Deep level photoluminescence of E50I2 peaks*
 (a) deep level 1: 1.28-1.04eV, (b) deep level 2: 0.90-0.71eV,
 (c) deep level 3: 0.66-0.46eV

The photoluminescence maps were made with a 1mm step in horizontal and vertical direction. The excitation laser trace was also ca. 1mm in diameter. For

comparison with resistivity and photoconductivity, a vertical profile of photoluminescence through the middle of the sample was made.

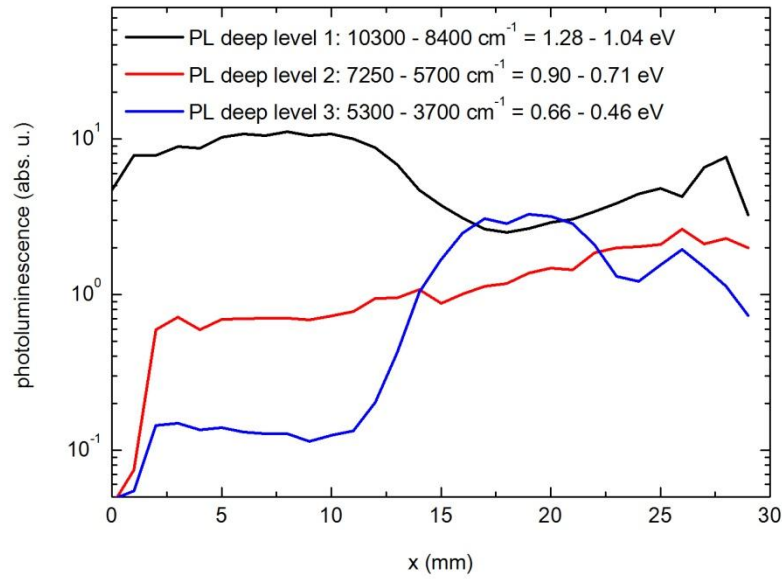


Fig. 46 *Photoluminescence profile of E50I2*

The profile shows that the luminescence of the deep level with highest energy ($1.28-1.04\text{eV}$) is most visible. All the signals have a small rise phase on the beginning of the sample. The PL intensity of the midgap level (deep level 2) increases throughout the whole sample. In closer look at the other two levels (deep level 1 and deep level 3), we can see that the PL intensities are in anti-correlation. It is mostly visible in the beginning of the sample, after the rise phase. Now we can compare **Fig. 43** with **Fig. 46**. As a helping tool, all the profiles have been recalculated as a fraction relative to the highest value in the profile and plotted into **Fig. 47**.

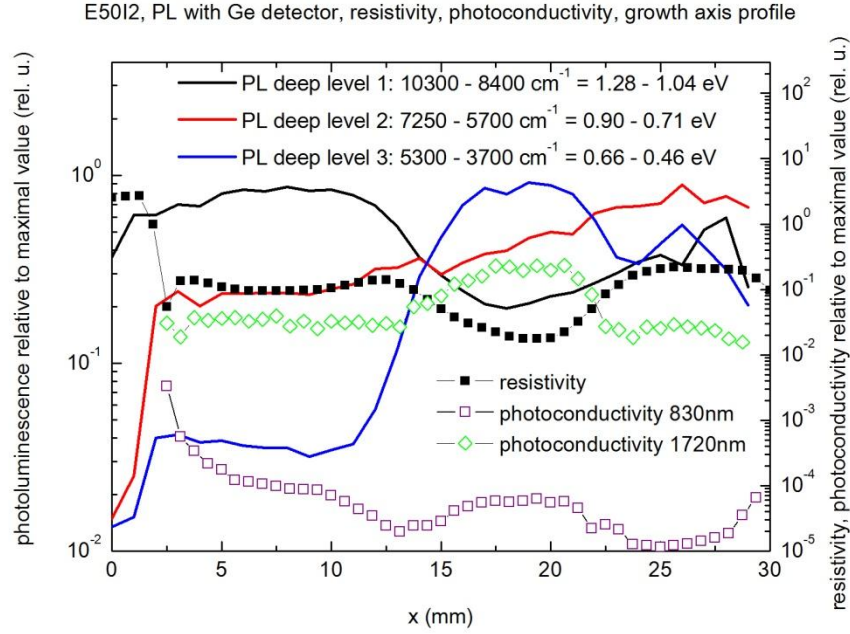


Fig. 47 *All measured parameters relative to their highest value in profile*

We can see that the intensity of photoluminescence of deep level 2 increases, but has little turns in the point where resistivity changes (approx. At $x=14$ and $x=22$). Meaning there can be a connection between the occupation of the midgap level and the resistivity as discussed above. But here also parameters of the other deep levels would have to be included in the theory.

In the first part of the sample the resistivity anti-correlates with the deep level 1 and correlates with deep level 3. Around the middle the trends are turned and resistivity starts to correlate with deep level 1 and anti-correlates with deep level 3. Since the photoconductivity with LEDs $1720nm$ almost fully anti-correlates with resistivity, the relation to the deep levels is reversal to their connection with resistivity. The photoconductivity with LEDs $830nm$ shows a part time correlation with deep level 1 (in the first half of the sample) and a correlation with deep level 3 (towards the end of the sample).

The connection between resistivity, photoconductivity and the deep level spectroscopy can be explained as above using the Fermi energy shift relative to the near to midgap deep level.

First we compare the measured energy levels with the ones described in Ref. [30]. Deep level 3 seems to be the level G (see Ref. [30]), which is $E_C - 0.64eV$.

The level lies in the upper half of the band gap. Deep level 2 ($E_V + 0.76\text{eV}$) seems to coincide with the level H . This is the near midgap level. The last level (deep level 1, $E_C - 1.1\text{eV}$) matches the level I .

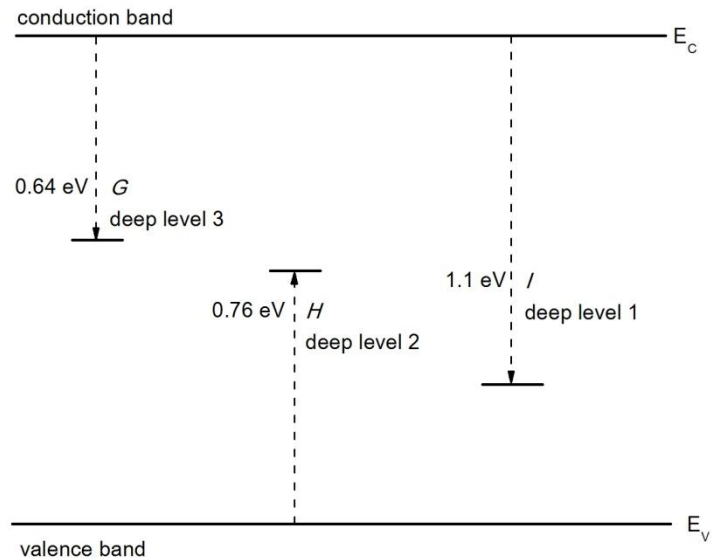


Fig. 48 Observed deep levels compared with levels described in Ref. [30]

In the region with the resistivity minimum (15-25mm, region with greatest parameter change) the concentration of deep level 3 rises. This changes the compensation conditions. As a result, the Fermi level shifts towards the conduction band. Due to the Fermi level shift the resistivity is lowered. A simple scheme of the process is shown in **Fig. 49**. The midgap level becomes more filled with electrons and therefore the photoluminescence transition between the conduction band and the midgap deep level 2 diminishes a little in this region. Increased filling factor of the midgap level also changes its trapping and recombination rates. Trapping of electrons is smaller and because of that the photoconductivity increases. Deep level 1 does not seem to have a direct connection to the profile in this region.

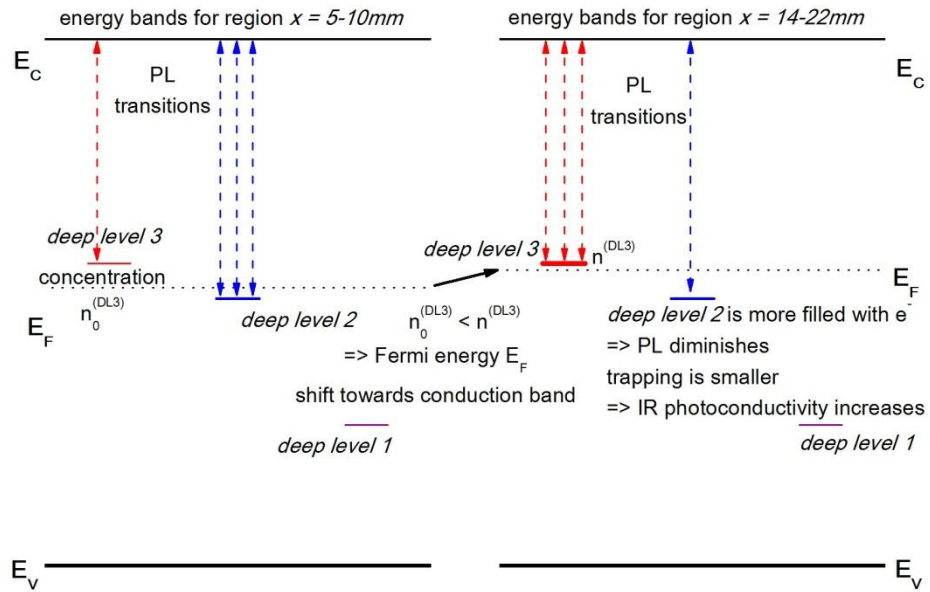


Fig. 49 Energy scheme of the Fermi level shift of sample E50I2

The parameter profiles for the sample E50I1 are shown in **Fig. 50**.

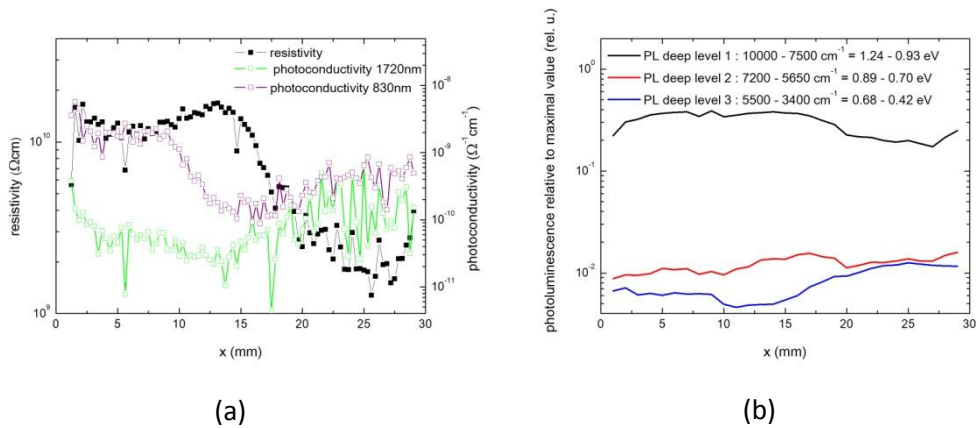


Fig. 50 Deep level spectroscopy on sample E50I1
 (a) Resistivity and photoconductivity profile
 (b) Deep level photoluminescence

Here the resistivity in the region $x=10-15mm$ rises. An inverse tendency relative to the sample E50I2 also supports the Fermi level shift theory. In the region with increased resistivity the photoluminescence of deep level 3 diminishes. The Fermi level shifts towards midgap, resistivity rises and the filling factor of deep level

2 is decreased (see **Fig. 51**). Therefore more transitions between the conduction band and the near midgap level take place and the photoluminescence increases. Trapping of electrons is higher and the photoconductivity decreases in this region.

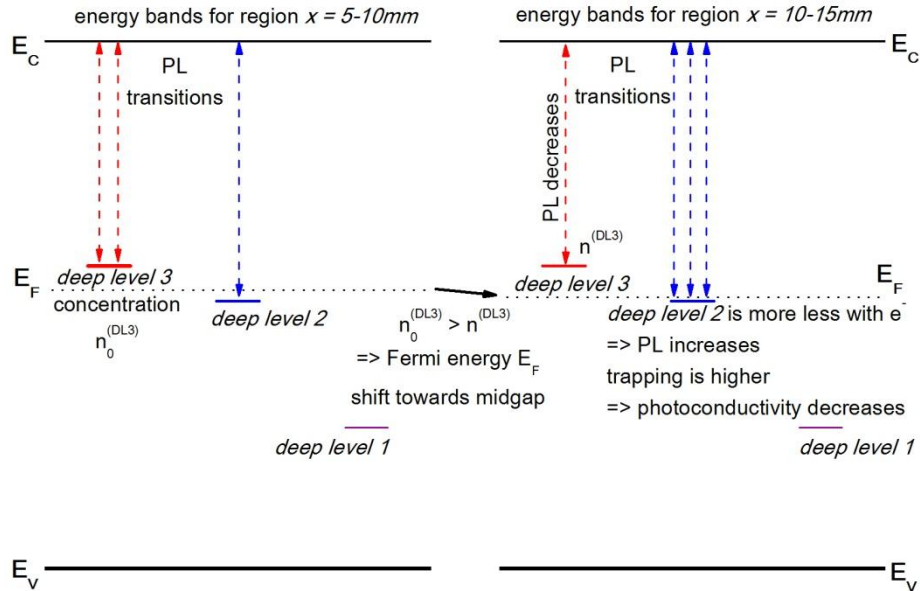


Fig. 51 Energy scheme of the Fermi level shift of sample E5011

Towards the end of the sample ($x=15-30\text{mm}$) the resistivity decreases. The evaluation of this region is the same as with the sample E5012. Photoluminescence of deep level 3 increases, the Fermi level shifts towards the conduction band. Photoluminescence of deep level 2 and photoconductivity decreases.

Deep level spectroscopy on samples grown in Prague was measured and compared in profile with resistivity and near midgap photoconductivity. Anti-correlation between resistivity and deep level 3 ($0.66-0.46\text{eV}$ on sample E5012, $0.68-0.42\text{eV}$ on sample E5011) photoluminescence was observed. Correlation between the IR photoconductivity and deep level 3 photoluminescence was also observed. Changes in the near midgap level photoluminescence (deep level 2, see **Table 10**) were observed in the region with greatest resistivity decrease/increase. The behavior between resistivity and photoconductivity profiles can be explained using the Fermi

level shift theory. Changes in the photoluminescence of deep levels support the used theory. Energy of the deep levels was compared to levels studied in [30].

5 Conclusion

The time-dependent charge measurement (TDCM) apparatus in FMF Freiburg was modified for application of a higher voltage source. Also the operating control of resistivity and photoconductivity measurement was upgraded.

A new set of LED for photoconductivity measurement with COREMA-WT was made.

Change in resistivity was observed depending on the frequency of the applied pulses in the measurement with commercial COREMA-WT. This phenomenon has been investigated through time delay and frequency dependency with TDCM in Freiburg.

Charge transport model using the Shockley-Read model with one deep level localized on the surface of the sample was calculated. This model did not seem to fit the measured tendencies of resistivity and other parameters.

Another theoretical model was developed, where the conductivity of the sample depends on the electric field. This assumption results in band bending on the sample surface and non-exponential behavior of the charge transport.

Changes of parameters, such as the dielectric relaxation time were observed in the time delay and frequency dependence measurement. The tendencies in both measurement sets fit the non-exponential behavior and can be explained with the theory presented.

Connection between resistivity and photoconductivity was investigated on VGF grown samples. Correlation and anti-correlation between these parameters was observed and explained using the theory of the Fermi level shift relative to a midgap deep level. This was supported with measured photoluminescence of this deep level.

Correlation and anti-correlation between measured deep level spectroscopy, resistivity and a near midgap photoconductivity was measured. Good correlation between photoluminescence peak of the deep level with energy around $0.5eV$ and infrared conductivity was observed. Correlated changes in the resistivity, photoconductivity and near midgap level photoluminescence were observed. Resistivity, photoconductivity and photoluminescence behavior was explained using the Fermi level shift theory.

6 References

- [1] R. B. James and T. E. Schlesinger, Semiconductors for room-temperature nuclear detector application, *San Diego: Academic Press, 1995*
- [2] V. Dědič, Fotoelektrický transport ve vysokoodporovém CdTe pro detektory Rentgenova záření (Photoelectric transport in high resistivity CdTe for gamma ray detectors), *Master Thesis, MFF UK, 2009*
- [3] COREMA-WT, Hardware User Manual, SemiMap Scientific Instruments GmbH, Tullastr. 67, 79108 Freiburg in Breisgau Germany
- [4] H. Elhadidy, J. Franc, P. Moravec, P. Höschl, and M. Fiederle, Deep level defects in CdTe materials studied by thermoelectric effect spectroscopy and photo-induced current transient spectroscopy, *Semicond. Sci. Technol* **22**, p. 537-542, 2007
- [5] R. Soundararajan, K. G. Lynn, S. Awadallah, C. Szeles, and S. Wei, Study of Defect Levels in CdTe Using Thermoelectric Effect Spectroscopy, *Journal of Electronic Materials*, Vol. 35, No. 6, 2006
- [6] E. Y. Lee, R. B. James, R. W. Olsen, and H. Hermon, Compensation and Trapping in CdZnTe Radiation Detectors Studied by Thermoelectric Emission Spectroscopy, Thermally Stimulated Conductivity, and Current-Voltage Measurements, *Journal of Electronic Materials*, Vol. 28, No. 6, 1999
- [7] J. Crocco, H. Bensalah, Q. Zheng, F. Dierre, P. Hidalgo, J. Carrascal, O. Vela, J. Piqueras, and E. Dieguéz, Study of the Effects of Edge Morphology on Detector Performance by Leakage Current and Cathodoluminescence, *IEEE Transactions on Nuclear Science*, Vol. 50, No. 4, 2011, p. 1935-1941
- [8] P. Moravec, P. Höschl, J. Franc, E. Belas, R. Fesh, R. Grill, P. Horodyský and P. Praus, Chemical polishing of CdZnTe substrates fabricated from crystals grown by the vertical-gradient freezing method, *Journal of Electronic Materials*, Volume 35, Number 6, p. 1206-1213, 2006
- [9] A. Cavallini, A. Castaldini, D. Cavalcoli, B. Fraboni, Photocurrent and Surface Photovoltage Spectroscopy Investigations of CdTe-Based Compounds, *IEEE Trans. Nucl. Sci. Volume 54, Issue 5*, p. 1719-1722, 2007
- [10] T. E. Schlesinger, J. E. Toney, H. Yoon, E. Y. Lee, B. A. Brunett, L. Franks, R. B. James, Cadmium zinc telluride and its use as a nuclear radiation detector material, *Material Science an Engineering* **32**, 2001, p.103-189

- [11] Y. Cui, M. Groza, D. Hillman, A. Burger, and R. B. James, Study of surface recombination velocity of Cd_{1-x}Zn_xTe radiation detectors by direct current photoconductivity, *Journal of Applied Physics*, 2002, **92**(5): p. 2556-2560
- [12] R. Stibal, J. Windscheif and W. Jantz, Contactless evaluation of semi-insulating GaAs wafer resistivity using the time-dependent charge measurement, *Semicond. Sci. Technol.* **6** (1991) 995-1001
- [13] J. Zázvorka, Mapování elektrického odporu a fotovodivosti semiizolačního CdTe bezkontaktní metodou (Mapping of electrical resistivity and photoconductivity of semiinsulating CdTe by contactless method), *Bachelor Thesis, MFF UK, 2010*
- [14] W. Shockley and W. T. Read, Jr., Statistics of Recombinations of Holes and Electrons, *Physical Review Volume 87*, Number 5, 1952
- [15] R. N. Hall, Electron-Hole Recombination in Germanium, *Physical Review Volume 87*, 387-387 (1952)
- [16] J. Franc, P. Höschl, Fyzika polovodičů pro optoelektroniku I (Semiconductor physics for optoelectronics I), *lecture scriptum p.87-89, MFF UK, <http://alma.karlov.mff.cuni.cz/polovodice/>*
- [17] I. Pelant, J. Valenta, Luminiscenční spektroskopie I Objemové krystalické polovodiče (Luminescence spectroscopy I Bulk crystal semiconductors), *Academia, 2006*
- [18] G. F. Knoll, Radiation Detection and Measurement 3rd edition, *John Wiley & Sons, 2000*
- [19] Z. He, Review of the Shockley-Ramo theorem and its application in semiconductor gamma-ray detectors, *Nuclear Instruments and Methods in Physics Research A 463*, p. 250-267, 2001
- [20] J. E. Toney, B. A. Brunett, T. E. Schlesinger, and R. B. James, Photocurrent mapping as a probe of transport properties and electric field distributions in cadmium zinc telluride detectors, *IEEE Transactions on Nuclear Science*, 1997, **44**(4): p.1684-1691
- [21] J. Kopáček, Matematická analýza pro fyziky IV (Mathematical analysis for physicists IV), *Matfyzpress, 2003*
- [22] M. Fiederle, M. Sowinska, A. Fauler, JP. Konrath, K. W. Benz, P. Siffert, Search of a characterisation methodology of CdTe/CZT wafers for imaging, *IEEE Nuclear Science Symposium Conference Record, 2003*

- [23] V.Zajac, Poruchy limitující sběr náboje v semiizolačním CdZnTe (Defects limiting charge collection in semiinsulated CdZnTe), *Master Thesis, MFF UK, 2011*
- [24] J. Crocco, J. Franc, J. Zázvorka, P. Hlídaek, E. Dieguez, V. Babentsov, M. V. Sochinskyi, R. B. James, Semi-Insulated Cd_{1-x}Zn_xTe Grown by the Vertical Gradient Freeze Method, *submitted to IEEE Trans. on Nucl. Science*
- [25] M. Zanichelli, M. Pavese, A. Zappettini, L. Marchini, N. Auricchio, E. Caroli, and M. Manfredi, Characterization of Bulk and Surface Transport Mechanisms by Means of the Photocurrent Technique, *IEEE Trans. Nuc. Sci., vol. 56, no. 6, pp. 3591-3596, 2009*
- [26] J. Kubát, J. Franc, V. Dědič, E. Belas, P. Moravec, V. Babentsov, P. Höschl, R. Grill, Photoconductivity mapping of semi-insulating CdTe, *IEEE Trans.Nucl.Sci.vol 58, pp.1953 2011*
- [27] J. Kubát, Fotoelektrický transport ve vysokoodporovém CdTe (Photoelectric transport in high resistivity CdTe), *Doctoral Thesis, MFF UK, 2011*
- [28] V.Babentsov, J.Franc, R.James, Compensation and photosensitivity in CdTe doped with In, *IEEE Trans.Nucl.Sci. vol.56, pp.1724, 2009*
- [29] V.Babentsov, J.Franc, R.James, Compensation and carrier trapping in indium-doped CdTe, Contributions from an important near-mid-gap donor, *Appl.Phys.Lett., vol.94, Art. No. 052102, 2009*
- [30] A. Castaldini, A. Cavallini, B. Fraboni, P. Fernandez, J. Piqueras, Deep energy levels in CdTe and CdZnTe, *Journal of Applied Physics Volume 83, Number 4, 1998, p. 2121-2126*

7 List of Tables

Table 1	<i>Properties of CdTe at 300K</i>
Table 2	<i>Properties of diode L3989</i>
Table 3	<i>Properties of diode ELD-1720-535</i>
Table 4	<i>Detector types and parameters in the PL measurement</i>
Table 5	<i>Frequency dependence of E50I1, dot1</i>
Table 6	<i>Samples used for resistivity, time delay and frequency dependency measurement</i>
Table 7	<i>Dependencies and relative changes of measured parameters on all used samples; I-increasing, D-decreasing, S-partially stagnating</i>
Table 8	<i>Tendencies and relative changes of parameters; I-increasing, D-decreasing, S-partially stagnating</i>
Table 9	<i>Samples used for resistivity, photoconductivity and deep level spectroscopy measurement</i>
Table 10	<i>Deep levels observed in the photoluminescence measurement</i>

8 List of Symbols and Abbreviations

N_t	Concentration of deep level
E_t	Energy of deep level
S_e, S_h ¹⁵	Trapping cross-section for electrons, holes
n_t	Trapped electrons concentration on the deep level
n, p	Concentration of free electrons, holes
v_e	Speed of electron
α_e	Thermal release probability of electron
E_F	Fermi energy
f	Fermi-Dirac distribution
k	Boltzmann constant ($k = 1.38 \cdot 10^{-23} J \cdot K^{-1}$)
T	Temperature
N_C	Number of states in conduction band
G	Charge generation rate
N_A, N_D, N_{DL}	Concentration of shallow acceptor, shallow donor and deep level
$\tau_r, \tau_{nr}, \tau_g$	Radiative, non-radiative and general electron lifetime
j	Current density
e	Elemental charge ($e = 1.602 \cdot 10^{-19} C$)
μ_n	Electron mobility
E	Electric field
σ_n	Conductivity for electron
Φ	Photon flow
η	Absorption ratio
w, A	Depth and Area
U	Voltage
Q	Charge
C	Capacity
R	Resistance
I	Current

¹⁵ Every abbreviation with index p marks the same parameter, only for holes instead of electrons

ρ	Resistivity
ϵ_0, ϵ_r	Vacuum and relative permittivity
γ	Photoconductivity
λ	Wavelength
α	Screening parameter
IR conductivity	Photoconductivity with LED wavelength 1720nm illumination
PL	Photoluminescence
Fig. #	Figure #
(#)	Equation #
Ref. [#]	Reference #